Highly reconfigurable neuron-mimicking conductive networks through nanophase structure engineering

Wei Zhong[1,#], Haojie Zhao[1,#], Bowen Yao[1,#,*], Zhenze Li[2], Zhifeng Wang[3], Yuhao Geng[1], Wen Sun[1], Jiajun Fu[1,*]

[1]School of Chemical Engineering, Nanjing University of Science and Technology, Nanjing, China, 210094.
[2]Department of Precision Instrument, Tsinghua University, Beijing, China, 100084.
[3]Testing Center, Yangzhou University, Yangzhou, China, 225002
[*]Corresponding Authors: B. Y. (e-mail: bowenyao@njust.edu.cn) or J. F. (e-mail: fujiajun668@njust.edu.cn).
[#]These authors contribute equally

Table of Contents

Supplementary Video 2 | The CP-PVA organogel-based electroluminescent devices.

Supplementary Video 3 | The CP-PVA organogel-based circuitry model for audio playing.

Supplementary Methods and Characterizations

Electrical conduction measurement

The sheet resistance (Rs) of CP-PVA hydrogels (2.5×2.5 cm^2) was measured using a four-point probe method with a digital source meter (2450 Graphical SourceMeter, Keithley, U.S.). The four-point probe used here adopted a linear configuration with a needle spacing of 1.59 mm. For conductance measurement, the probe was directly attached to the surface of the gel samples. Then, a constant current was applied to the outer two probes and the voltage difference between the inner two probes was measured. The sheet resistance (Rs), resistivity (ρ), and conductivity (σ) were therefore calculated according to the following equation by using the thickness obtained by an optical profilometer (ContourGT-X, Bruker, U.S.) (Equations 1, 2, and 3):

$$R_s = \frac{\mathrm{V}}{\mathrm{I}} \quad \text{(Equation 1)}$$

$$\rho = R_s \times T \times 4.38 \quad \text{(Equation 2)}$$

$$\sigma = \frac{1}{\rho} \quad \text{(Equation 3)}$$

where I, V, Rs, and T are the current, voltage, resistance, and thickness, respectively.

Interface impedance measurement

The interfacial impedance between the CP-PVA organogels and skin was measured using an electrochemical workstation (CHI660E, CH Instruments, U.S.). Two pieces of the CP-PVA organogel (the active area in contact with the skin was a circular region with a diameter of 1.5 cm) were placed on the forearm side by side with a central distance of 2 cm, then connected to an electrochemical working station (CHI660E, CH Instrument, U.S.). Electrochemical impedance spectra were obtained at an initial potential of 0 V (vs. CP-PVA organogel reference) with a 5 mV AC amplitude over a frequency range of 10^5 to 10^{-1} Hz.

Attenuated total reflectance Fourier-transform infrared (FT-IR) spectra analysis

Fourier-transform infrared (FT-IR) spectra were performed by a spectrometer (Tensor II, Bruker, U.S.) equipped with attenuated total reflectance (ATR). For the FT-IR tests, the samples were pressed against the high-refractive-index crystal mounted on the FT-IR spectrometer with a universal compression force of 80 N. The FT-IR spectra were recorded over the wavelength range of 700–4000 cm^{-1}, with scan numbers of 16 and a resolution of 4 cm^{-1}. Temperature-dependent FT-IR spectra were measured with GoldenGate ATR accessory (MK II, Specac Company, U.K.), and the temperature was controlled in a range of 20-140 °C with an interval of 10 °C.

UV-vis transmittance spectra analysis

An appropriate volume of the CP–PVA precursor solution (containing 7.4 mg mL^{-1} of CP and 26.1 mg mL^{-1} of PVA, with 4 wt% glycerol relative to the total solution mass) was spin-coated onto a quartz glass (2 cm in length, 2cm in width) substrate at a speed of 500, 700, 900, 1100, 1300, 1500 rpm. The coated substrate was then left to dry at ambient temperature (25 °C) to remove excess water. To improve the conductance, a further thermal annealing process was implemented at 80 °C for 2 h. Then, the UV-vis transmittance spectra were obtained by a UV-vis spectrophotometer (Evolution 220, Thermo Scientific, U.S). The studied range was set to 350–1000 nm with 0.5 nm step width.

XRD patterns analysis

The structural and crystalline characteristics of CP-PVA organogel were obtained through X-ray diffraction (XRD) spectroscopy (D/MAX-2500V/PC, Rigaku Corporation, Japan) using copper Kα radiation (k=1.54056 Å). The test conditions were as follows: tube flow 100 mA, tube pressure 40 kV, steplength was 2θ= 0.02°, and 2θ range was 10° to 80°.

SAXS analysis

The CP – PVA organogel was precisely cut into specimens measuring 5 mm × 5 mm, which were subsequently stacked to a total height of approximately 1 mm to achieve the optimal thickness for characterization. To preserve structural integrity and minimize potential contamination, the stacked specimens were secured using 3M testing tape.

The MetalJet X-ray source (Excillum D2+) with a liquid metal anode was operated at 70 kV and 3.57 mA, emitting Ga-Kα radiation with a wavelength of λ = 1.314 Å. The sample-to-detector distances ranged from 0.5 to 1.7 m, covering the scattering vector q range from 0.007 to 0.2 $Å^{-1}$ (q is the scattering vector, $q = (4\pi/\lambda)\sin(\theta)$, where 2θ represents the scattering angle). The SAXS patterns were normalized to an absolute scale and azimuthally averaged to obtain the intensity profiles, and the empty cell as the background was subtracted. The approach used to evaluate the SAXS data applies a set of general laws (Porod's law, Guinier analysis) that yield results right after data reduction. Then the scattering curves were fitted with models that yield accuracy parameters for data analysis.

Raman spectrum analysis

Each sample was pressed between a glass slide and a coverslip to ensure a flat surface. Raman spectrum was obtained the confocal Raman microscope (alpha300 RA, WITec, Germany) equipped with a 20× objective (LSM 980, Zeiss, Germany) was utilized for the measurements. An Nd: YAG laser (532 nm) with a maximum power of 75 mW served as the excitation source. Data were collected using a charge-coupled device detector (DU401A-BV, Andor, UK) behind a grating spectrometer (UHTS 300, WITec, Germany).

Surface topography analysis

Firstly, the glycerol suspensions (4 wt%, relative to the total mass of solution) containing 7.4 mg mL^{-1} of CP and 26.1 mg mL^{-1} of PVA (CP's relative content: 22 wt%) were spin-coated onto Indium-Tin Oxide conductive film glass (2 cm in length and 2 cm in width) substrate at a speed of 500 rpm. The coated substrate was then left to dry in an ambient environment (25 ℃) to evaporate the excess water. The p-CP-PVA organogel was thermally treated at 80°C for 2 hours to obtain conductive CP-PVA. Then the surface topography, phase images, and tunneling current image in mode maps of the CP-PVA organogels are measured using an atomic force microscope (Dimension Icon, Bruker, U.S.) in tapping mode. The conducting probe lightly taps on the sample surface with a recorded phase shift angle of the probe motion relative to a driving oscillator, whereas a constant 3 V bias is applied to the sample, and the contact current value is evaluated. The bright regions with high phase angles correspond to regions with relatively high modulus, and the dark regions with low phase angles correspond to regions with relatively low modulus.

The influence of thermal diffusion triggered by laser irradiation on the interfacial region was thoroughly examined. Specifically, laser irradiation was applied to partially irradiate one-half of the CP–PVA organogels. Subsequently, the surface topography, phase images, and tunneling current image maps of the interfacial area are measured using an atomic force microscope in tapping mode.

Solid content tests

The CP-PVA organogels were immersed in deionized water until no glycerol in the gels. The gels were then freeze-dried to constant weights. The solid content (C_S) of the CP-PVA organogels was calculated using the following equation (Equation 4).

$$C_S = \frac{W_R}{W_0} \times 100\% \qquad \text{(Equation 4)}$$

where W_R and W_0 are the masses of the CP-PVA organogel at fully dried and pristine states, respectively.

Mechanical tensile tests

Uniaxial tensile tests were conducted using a tester (AGS-X, Shimadzu, Japan) at a strain rate of 200% min^{-1}

at ambient temperature (25 °C). The CP-PVA organogels were cut into a dog-bone shape (25 mm in length, 10 mm in width, 75 μm in thickness) and were employed for tests. And securely held with the insulative clamps of the tensile tester. Then, the specimen was stretched at a strain rate of 200% min^{-1}. Stress-strain curves were obtained by dividing the measured force by the initial cross-sectional area and the measured displacement by the initial clamping distance. Four gel samples were tested for each condition.

In situ resistance measurement upon strain

For resistance change measurement of CP-PVA organogels upon strain, CP-PVA organogels were cut into a dog-bone shape (25 mm in length, 10 mm in width, 75 μm in thickness) and were employed for tests. The two ends of the specimens were first electrically connected to a digital source meter (2450 Graphical SourceMeter, Keithley, U.S.) through adhesive copper strips previously coated with a thin player of silver paste for reduced contact resistance, and then securely held with the insulative clamps of tensile tester (AGS-X, Shimadzu, Japan). Then, the specimen was cyclically stretched in the range of 0%-50% of its original length at a strain rate of 200% min^{-1}, during which the resistance change with strain was measured by applying a constant current (100 μA) at a sampling rate of ~5 Hz.

The in situ resistance measurement upon strain and cyclically stretched of the laser-irradiated CP-PVA organogels and soldered CP-PVA organogel samples (with themselves and metal) were also measured using the same method.

Stability analysis

The CP-PVA organogels/hydrogels were placed in a smart temperature and humidity-controlled chamber (Thermotron SM-3.0, Keyuete Technology, China) set at three different temperatures (40°C, 60°C, and 80°C) and two humidity levels (15% and 45%) for 7 hours. During the experiment, the weight and resistance of the gel were recorded at regular time intervals to monitor changes. Additionally, the Uniaxial tensile tests of the gel were tested and compared at various time points to evaluate the impact of temperature and humidity on its mechanical performance.

Measurement of adhesion performance

The CP-PVA organogels at State III were fixed at 20 mm × 10 mm × 75 μm length×width×thickness). A nylon tape was bonded to the upper surface of the CP-PVA organogel as a rigid backing to prevent any plastic deformation of the hydrogel during the tests. In detail, for soldering, CP-PVA organogels at State III were coated with a thin layer of sans-glycerol CP/PVA aqueous solution (7.4 mg mL^{-1} of CP and 26.1 mg mL^{-1} of PVA, mass loading: 10 μL cm^{-2}), gently pressed against the targeted adherend (5 kPa), selectively dried overnight (for mechanical bonding), and then thermally annealed at 80 °C (for electrical connect). The CP-PVA was successfully bonded to the targeted adherend. For metal substrates, a 5-minute oxygen plasma treatment was applied to improve hydrophilicity. The samples were then securely held with insulated clamps in the tensile tester (AGS-X, Shimadzu, China) and stretched at a strain rate of 200% min^{-1}. All 90° peel tests were performed at a loading rate of 200% min^{-1}. The interfacial toughness (Γ) was quantified using the following empirical equation (Equation 5).

$$\Gamma = Fs/W \qquad \text{(Equation 5)}$$

where Fs is the steady-state peeling force, and W is the width of the organogels.

Physiological signal capturing

Electrophysiological signals were recorded using a biosignal acquisition system (Cyton board, OpenBCI, U.S.). For electrocardiogram (ECG) signal acquisition, three independent CP-PVA organogel electrodes were placed on the right-hand index finger, left-hand index finger, and right-hand middle finger, serving as the negative, positive, and ground electrodes, respectively. For skin surface electromyography (EMG) tests, multi-electrode arrays (channel counts: 8, the size of each electrode: 0.5 cm^2) were employed and attached

to the upper arms to map the distribution of EMG activities of target muscles, with a common ground electrode placed on the wrist. For electromyography (EMG) tests, 8-channel multi-electrode arrays (each electrode sized at 0.5 cm^2) were applied to the upper arms to map the EMG activity distribution of target muscles, with a common ground electrode positioned on the wrist. All the data were filtered through a bandpass filter $(2-49\ Hz)^2$.

Supplementary Note 1| Study on the mechanical performance of pristine CP-PVA organogels before thermal annealing (p-CP-PVA).

The mechanical properties of the pristine CP-PVA organogels before thermal annealing (p-CP-PVA) were highly dependent on the overall solid content and the relative contents of their components. To tune their solid contents, precursor solutions with different glycerol concentrations (1-10 wt%, relative to the total mass of suspension) were employed and p-CP-PVA organogels with different solid contents of 15%-86% were obtained (CP's content was controlled to be 22 wt%, relative to the total mass of PVA and CP). With the solid content decreasing from 86 wt% to 15 wt%, p-CP-PVA experienced a significant decrease in Young's modulus (from 145.2 MPa to 2.4 MPa) and fracture stress (from 50.8 MPa to 3.1 MPa), with a substantial increase in fracture elongation from 34% to 767%. An optimum toughness of as high as 71.4 MJ m^{-3} was achieved at the glycerol concentrations of 4 wt% (solid content: ~40 wt%) (Supplementary Fig. 2).

On the other hand, the effect of CP's content on mechanical performance was also studied. By regulating the concentration of CP in the precursor solutions (10 wt% to 34 wt%, relative to the total mass of CP and PVA), p-CP-PVA organogels with different content of CP were prepared (Supplementary Fig. 3). With the CP's content from 0 wt % increase to 34 wt%, Young's modulus of p-CP-PVA organogels increased significantly from 2.0 MPa to 13.5 MPa, while the fracture elongation first increased from 811% to 1047%, then decrease to 415%. Similarly, the fracture stress of p-CP-PVA organogels increases from 4.2 MPa to 11.4 MPa and then decreases to 8.2 MPa, thus leading to an optimum toughness of as high as 71.4 MJ m^{-3} at the relative content of CP of 22 wt%.

Supplementary Note 2 | Effect of thermal annealing on the electrical and mechanical performances of CP-PVA organogels.

The pristine CP-PVA organogels (p-CP-PVA) exhibited low conductivities (Supplementary Fig.4). To enhance their conductance, thermal annealing was implemented. Overall, the conductance of organogel after thermal annealing showed a positive relationship with annealing temperature (Supplementary Fig. 5a). For the CP-PVA organogel prepared from a precursor solution containing 22 wt% of CP (relative content to the total mass of PVA and CP) and 4 wt% of glycerol (relative to the total mass of precursor solution), increasing the annealing temperatures from 30 °C to 80 °C led to dramatic improvements in the conductivity from 4.5×10^{-4} S cm^{-1} to 27.3 S cm^{-1} (the annealing time was fixed at 2 hours) (Supplementary Fig. 5c). Meanwhile, due to the low volatility of glycerol, the organogel well remained in the gel states, with only a few increases in solid contents from ~40 wt% to ~51 wt% mainly corresponding to the water evaporation (Supplementary Fig. 5b). However, a further increase in annealing temperature (*e.g.*, 100 °C) would lead to substantial glycerol loss, despite with a higher conductance of 29.7 S cm^{-1} (Supplementary Fig. 5a). Therefore, given the balance between the high conductance, controllability, and stability of the organogel system, thermal annealing of 80 °C was adopted in this work.

CP-PVA organogels underwent slight changes in mechanical properties after thermal annealing. Specifically, Young's modulus, toughness, and fracture stress increased by 11.4% (from 10.3 MPa to 12.1 MPa), 13.3% (from 71.4 MJ m^{-3} to 82.4 MJ m^{-3}), and 50.5% (from 11.1 MPa to 16.7 MPa), respectively, while the fracture elongation decreased by 22.4% (from 845% to 656%) (Fig. 2c, d and Supplementary Fig. 3, 7). These changes suggest that thermal annealing had a moderate effect on improving the rigidity and strength of the CP-PVA organogels, with a minor reduction in their flexibility.

Supplementary Note 3 | Effect of the thickness of CP-PVA organogels on their electrical performances.

Semi-transparent conductive organogels with different thicknesses were prepared by spin-coating precursor solutions containing PVA, CP, and glycerol (CP's content: 22 wt%, relative to the total mass of CP and PVA; glycerol's content: 4 wt%, relative to the total mass of precursor solution), followed by thermal annealing at 80 °C for 2 hours. The semi-transparent conductive organogels showed good conductivity (29.7 to 34.7 S cm^{-1}, depending on the thickness of organogels) close to that of bulk organogels prepared by drop-casting (thickness: 75 μm, conductivity: 27.3 S cm^{-1}), indicating the conductive network was uniformly distributed in the organogel matrix (Supplementary Fig. 6). In addition, the slight dependency of conductivity on the thickness probably originated from the difference in the solid contents of the organogels with different thicknesses (though the precursor solution used were the same), given the evaporate kinetics during thermal annealing.

Supplementary Note 4 | Environmental stability of CP-PVA organogels.

Compared with hydrogels, glycerol-based organogels demonstrated excellent stability in ambient environments and high resistance to high temperatures (40-80 °C), greatly boosting the reliability and temperature window of the gel system. As controls, conductive hydrogels were prepared by dialyzing the conductive organogels in water, followed by drying at 80 °C and reswelling in purified water. The hydrogels dehydrated quickly even at a mild temperature of 40 °C as revealed by a sharp loss of ~ 92% in weight within 4 hours, accompanied by embrittlement with increased Young's modulus (Supplementary Fig. 10-12). By contrast, the glycerol-based organogels remain nearly stable at high temperatures up to 80 °C at different humidity (*e.g.,* 15% and 45%) (Supplementary Fig. 16-17). For example, after exposure to a high-temperature environment (80 °C) with low humidity (15%) for 7 hours, the organogels experienced slight dehydration (weight loss: 11.4%), with small decreases of 9.5% and 19% in resistance and fracture strain (644% to 522%), respectively.

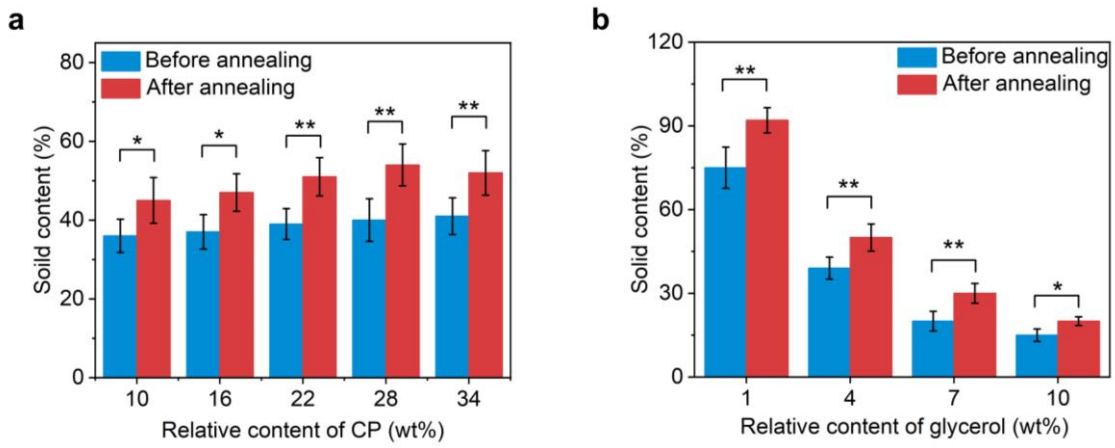

Supplementary Fig. 1 | Solid contents of CP-PVA organogels before and after thermal annealing. a, The solid contents of CP-PVA organogels with different relative contents of CP ranging from 10 wt% to 34 wt% (relative to the total mass of CP and PVA). The relative contents of glycerol in the precursor suspension used for the preparation of these CP-PVA organogels were fixed to be 4 wt%. **b,** The solid contents of CP-PVA organogels could be controlled by varying the glycerol's relative contents in the precursor solutions used for the preparation of these CP-PVA organogels (relative to the total mass of the precursor suspension). The relative contents of CP were fixed to be 22 wt%, relative to the total mass of CP and PVA. The data in **a** and **b** are presented as mean values ± standard deviation (s.d.), with four samples tested in independent measurements. Statistical significance was assessed using two-sided *t*-tests for comparisons between two groups (panels **a** and **b**) with significance levels denoted as $p \geqslant 0.05$ (not significant, NS), $p < 0.05$(*), $p < 0.01$(**), and $p < 0.001$(***).

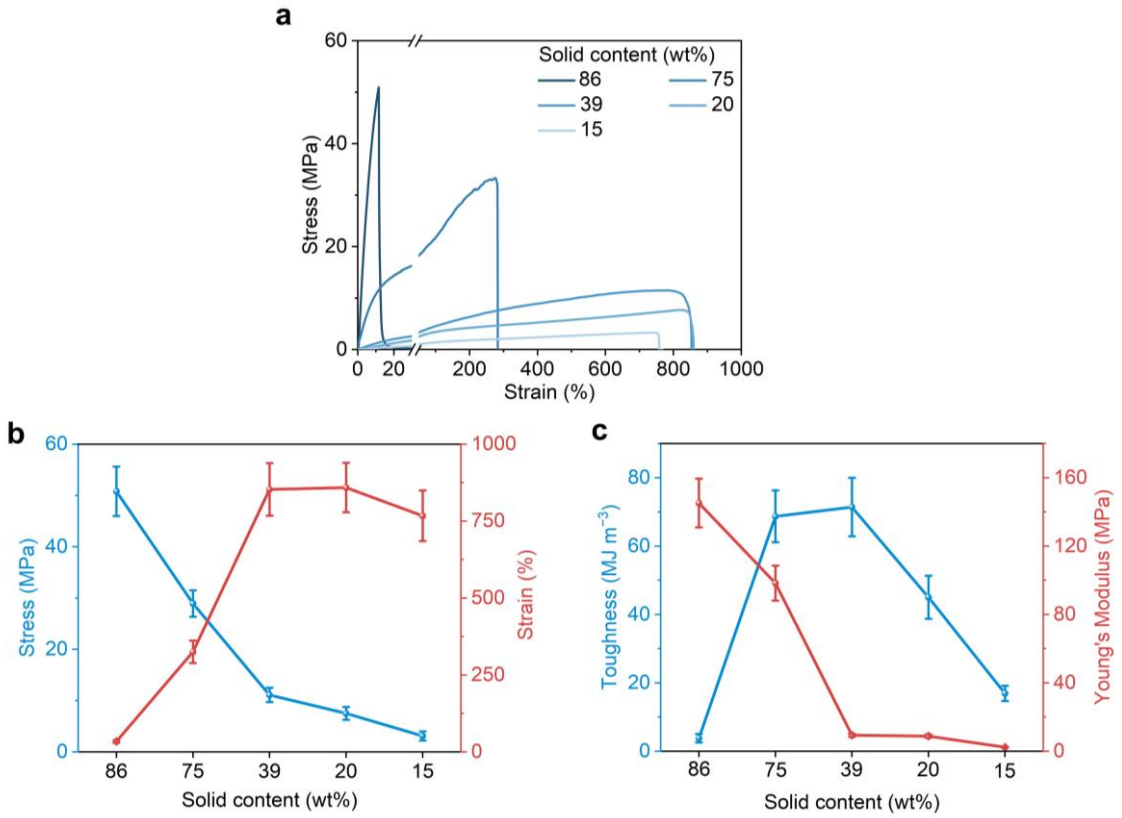

Supplementary Fig. 2 | Mechanical properties of pristine CP-PVA organogels (p-CP-PVA). a, Stress-strain curves of p-CP-PVA organogels with different solid contents at a strain rate of 200% min^{-1}. **b, c,** Comparison of Young's modulus, fracture stress, and fracture strain of p-CP-PVA organogels with different solid content. The solid contents of organogels were tunned by controlling the glycerol concentration in the precursor solutions used for the preparation (1-10 wt%, relative to the total mass of precursor solution). The relative contents of CP in the CP-PVA organogels were fixed to be 22 wt% (relative to the total mass of CP and PVA). The data in **b** and **c** are presented as mean values ± standard deviation (s.d.), with four samples tested in independent measurements.

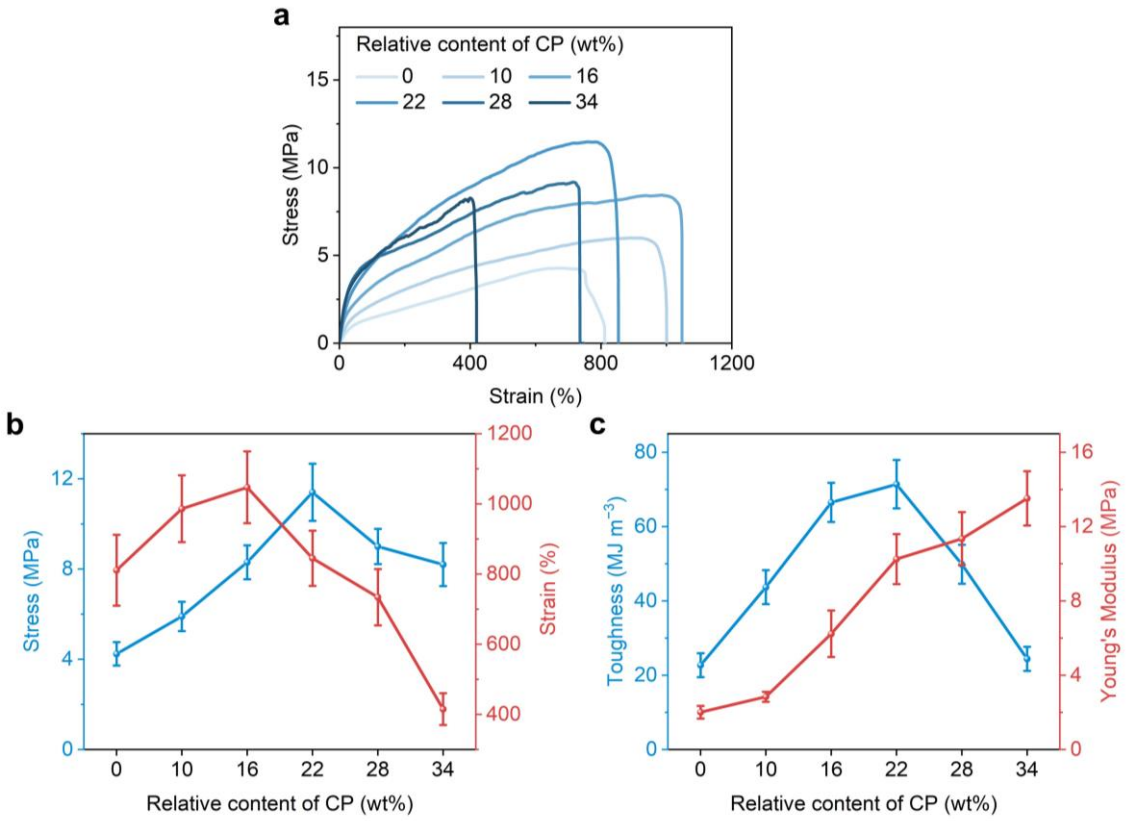

Supplementary Fig. 3 | Mechanical properties of p-CP-PVA organogels with different contents of CP. **a,** Tensile stress-strain curves of p-CP-PVA organogels recorded at a strain rate of 200% min^{-1}. The contents of CP varied from 10 wt% to 34 wt% (relative to the total mass of CP and PVA). **b, c,** Comparison of fracture stress, fracture strain, toughness, and Young's modulus of the CP-PVA organogels with different contents of CP. The data in **b** and **c** are presented as mean values ± standard deviation (s.d.), with four samples tested in independent measurements.

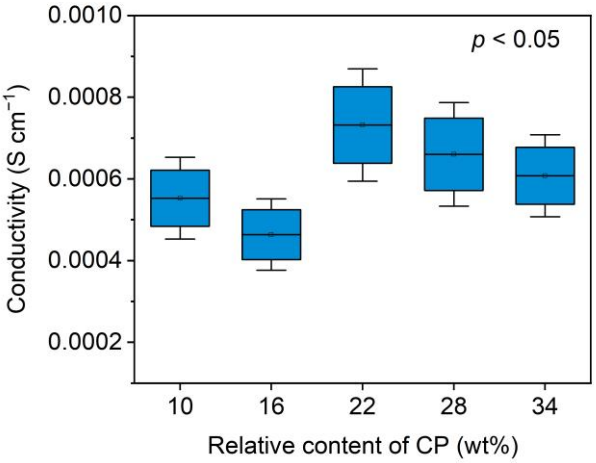

Supplementary Fig. 4 | Conductivities of p-CP-PVA organogels with different contents of CP. The p-CP-PVA organogels had relative contents of CP in a range of 10 wt%-34 wt% (relative to the total mass of CP and PVA), with solid contents of 36 wt%-41 wt%. The conductivities were measured using a four-point probe method with a digital source meter. The data are presented as mean ± standard deviation (s.d.) from four independent samples. The data are presented in box-and-whisker plots, where the central dots, lines, and box limits indicate the mean, the median, and the upper/lower quartiles, and the whiskers extend to 1.5× the interquartile range from the quartiles. Statistical significance was assessed using one-way analysis of variance (ANOVA) for comparisons among multiple groups, with significance levels denoted as $p \geq 0.05$ (not significant, NS), $p < 0.05$(*), $p < 0.01$(**), and $p < 0.001$(***).

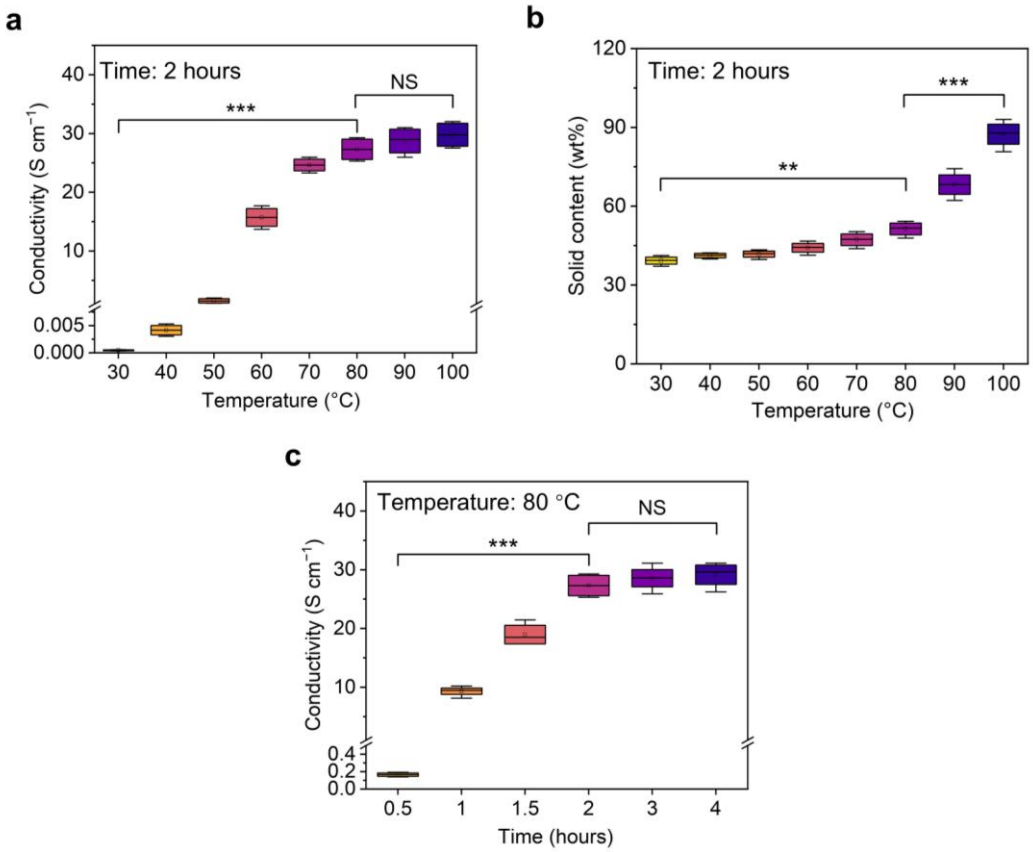

Supplementary Fig. 5 | The effect of thermal annealing on the conductivity of CP-PVA organogels. a, b, Conductivities and solid contents of CP-PVA organogels after being subjected to thermal annealing at 30-100°C for 2 hours. **c,** Conductivities of CP-PVA organogels after being subjected to thermal annealing at 80 °C for different times. The p-CP-PVA organogels (before annealing) used for the tests had solid contents of ~39 wt% (glycerol's content in the precursor suspension used for organogel preparation was 4 wt%) and CP's relative content of 22 wt% (relative to the total mass of CP and PVA). The data in panels **a**, **b,** and **c** are presented as mean ± standard deviation (s.d.) from four independent samples. The data in panels **a**, **b,** and **c** are presented in box-and-whisker plots, where the central dots, lines, and box limits indicate the mean, the median, and the upper/lower quartiles, and the whiskers extend to 1.5× the interquartile range from the quartiles. Statistical significance was assessed using two-sided *t*-tests for comparisons between two groups (panels **a**, **b,** and **c**), with significance levels denoted as $p \geq 0.05$ (not significant, NS), $p < 0.05$(*), $p < 0.01$(**), and $p < 0.001$(***).

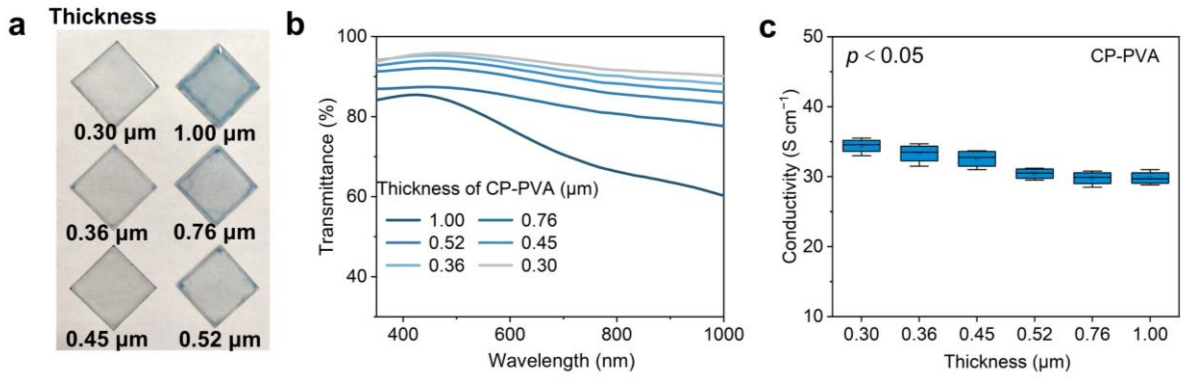

Supplementary Fig. 6 | Ultraviolet-visible (UV-Vis) spectra of semi-transparent CP-PVA organogels prepared through spin-coating. For the preparation of the semitransparent organogels, glycerol suspensions (4 wt%, relative to the total mass of solution) containing 7.4 mg mL^{-1} of CP and 26.1 mg mL^{-1} of PVA (CP's relative content: 22 wt%) were spin-coated on glass substrates at speed rates of 500 to 1500 rpm, followed by selective evaporation and thermal annealing at 80°C for 2 hours. **a,** The digital photographs of CP-PVA organogels with varied thicknesses of 0.3-1 μm. **b,** Transmission curves of CP-PVA organogels with varied thicknesses of 0.3-1 μm. **c,** The conductivity of CP-PVA organogels with different thicknesses. The data in panel **c** are presented as mean ± standard deviation (s.d.) from four independent samples. The data in panel **c** are presented in box-and-whisker plots, where the central dots, lines, and box limits indicate the mean, the median, and the upper/lower quartiles, and the whiskers extend to 1.5× the interquartile range from the quartiles. Statistical significance in panel **c** was assessed using ANOVA for comparisons among multiple groups (panel **c**), with significance levels denoted as $p \geq 0.05$ (not significant, NS), $p < 0.05$(*), $p < 0.01$(**), and $p < 0.001$(***).

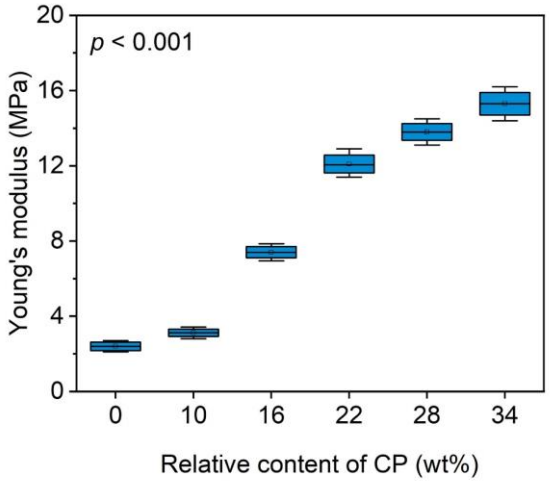

Supplementary Fig. 7 | Young's modulus of the CP-PVA organogels with different contents of CP. The Young's modulus was calculated from the tensile stress-strain curves of CP-PVA organogels shown in Fig. 2c in the main manuscript. The solid contents of the CP-PVA organogels were ~50 wt% (glycerol's content in the precursor suspension used for the organogel preparation was 4 wt%). The data are presented as mean ± standard deviation (s.d.) from four independent samples. The data are presented in box-and-whisker plots, where the central dots, lines, and box limits indicate the mean, the median, and the upper/lower quartiles, and the whiskers extend to 1.5× the interquartile range from the quartiles. Statistical significance was assessed using ANOVA for comparisons among multiple groups, with significance levels denoted as $p \geq 0.05$ (not significant, NS), $p < 0.05$(*), $p < 0.01$(**), and $p < 0.001$(***).

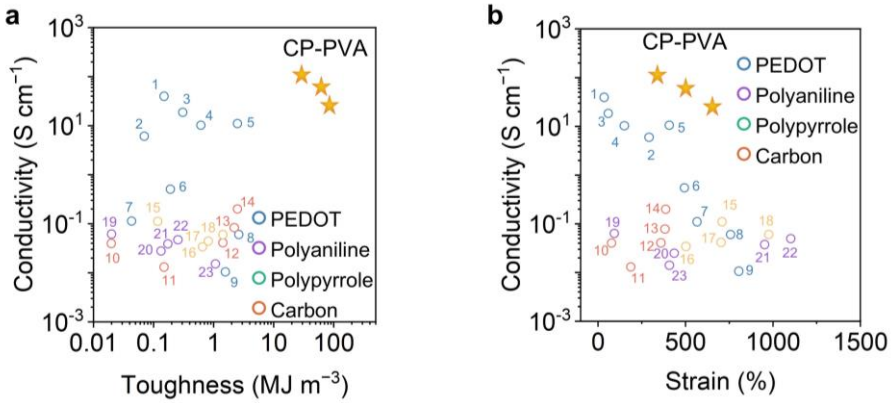

Supplementary Fig. 8 | Ashby plot comparing the toughness, strain, and conductivity of CP-PVA organogels with previously reported conducting polymer hydrogels/organogels. The data points are obtained from references mentioned in Supplementary Table 1.

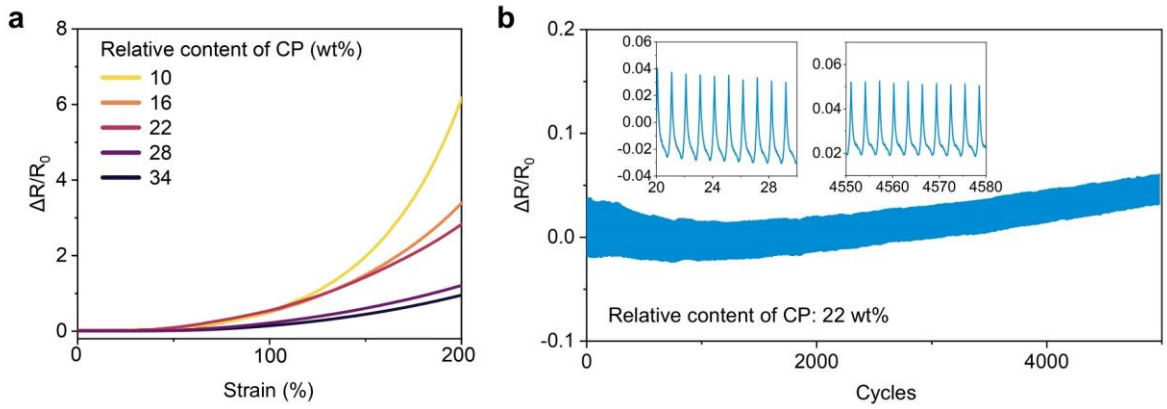

Supplementary Fig. 9 | Resistance changes of organogels upon tensile strain. a, Resistance change (ΔR/R0) of CP-PVA organogels with different relative content of CP (relative to the total mass of CP and PVA) upon tensile strains. The solid contents of the thermally-annealed CP-PVA were ~50 wt% (glycerol's content in the precursor suspension used for the organogel preparation was 4 wt%). **b,** Resistance change ($\Delta R/R_0$) of the CP-PVA organogel with CP's contents of 22 wt% upon cyclic stretching with a strain range of 0-50% for 5,000 cycles.

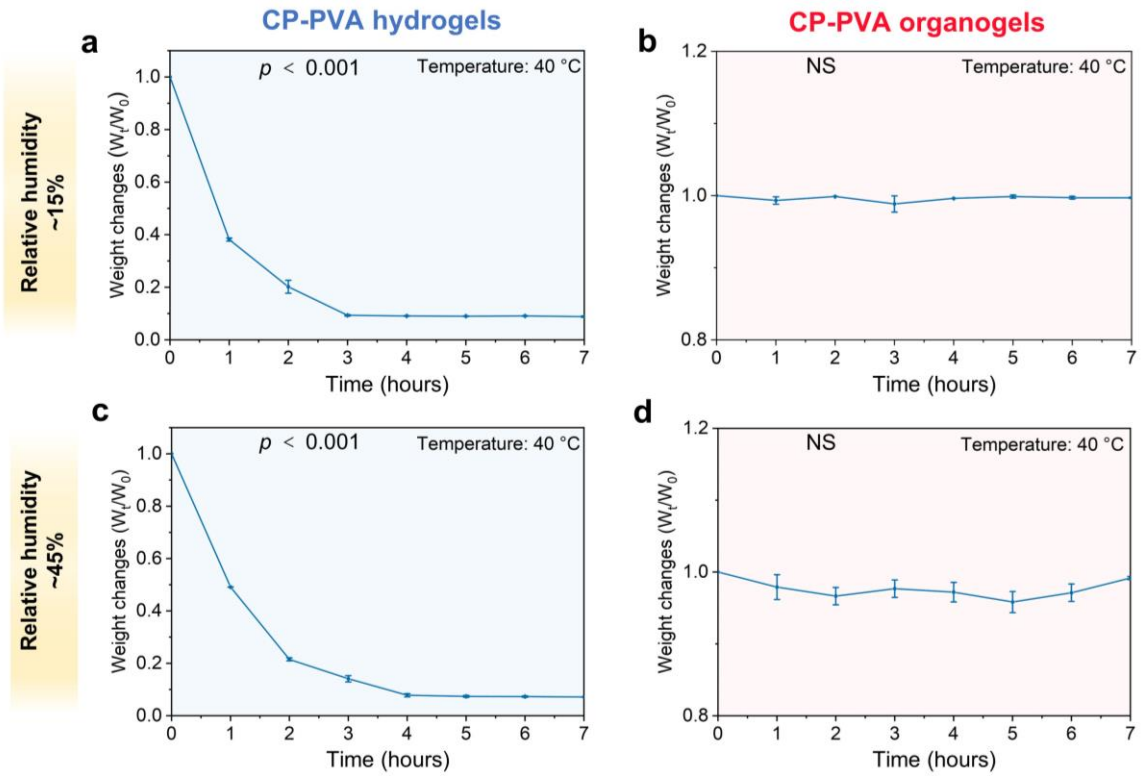

Supplementary Fig. 10 | Weight changes of CP-PVA hydrogels and CP-PVA organogels at 40 °C. a-d, Weight changes (W_t/W_0) of CP-PVA hydrogels (**a, c**) and CP-PVA organogels (**b, d**) when subject to environments with low (**a-b**) and high humidity (**c-d**) at 40 °C, where W_t refers to the weights of the gels at different times and W_0 refers to the initial weights of the gels. The CP-PVA organogels, with a solid content of ~50 wt% and CP's relative content of 22 wt%, were used for experiments. The hydrogel counterparts were prepared by dialyzing the corresponding organogels in water, followed by drying at the ambient environment (25 ℃) and reswelling in purified water. The data in panel **a-d** are presented as mean values ± standard deviation (s.d.), with four samples tested in independent measurements. Statistical significance was assessed using ANOVA for comparisons among multiple groups (panel **a-d**), with significance levels denoted as $p \geq 0.05$ (not significant, NS), $p < 0.05$(*), $p < 0.01$(**), and $p < 0.001$(***).

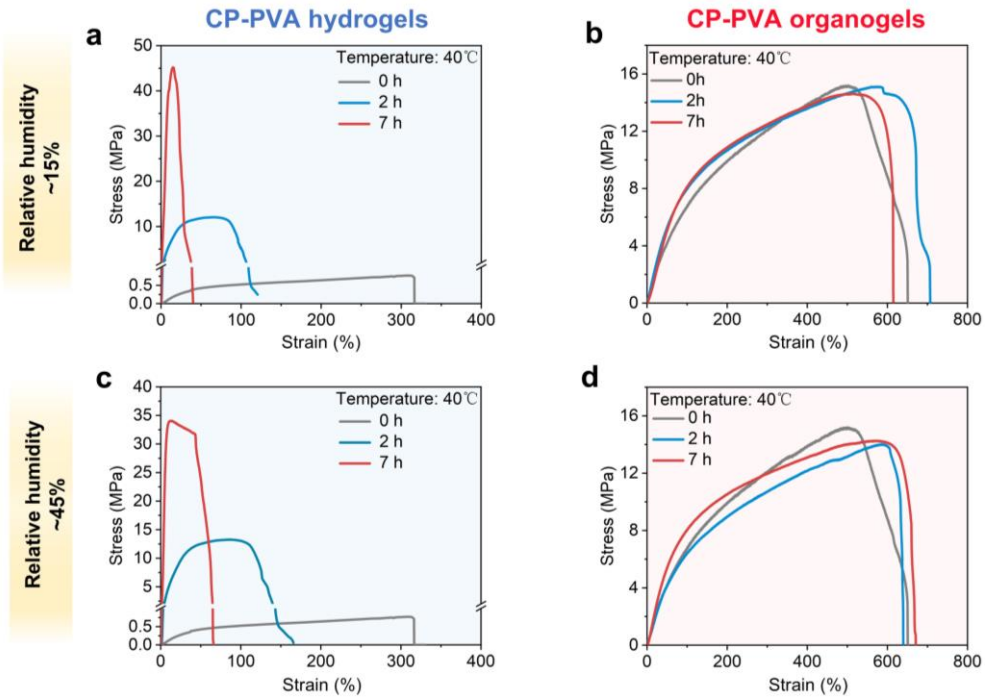

Supplementary Fig. 11 | The mechanical stability of CP-PVA hydrogels and CP-PVA organogels at 40 °C. a-d, Tensile stress-strain curves of CP-PVA hydrogels (**a, c**) and CP-PVA organogels (**b, d**) after being subjected to environments with low (**a, b**) and high humidity (**c, d**) at 40 °C for 7 hours. The stress-strain curves were recorded at a strain rate of 200% min^{-1}. The CP-PVA organogels, with a solid content of ~50 wt% and CP's relative content of 22 wt%, were used for experiments. The hydrogel counterparts were prepared by dialyzing the corresponding organogels in water, followed by drying at the ambient environment (25 °C) and reswelling in purified water.

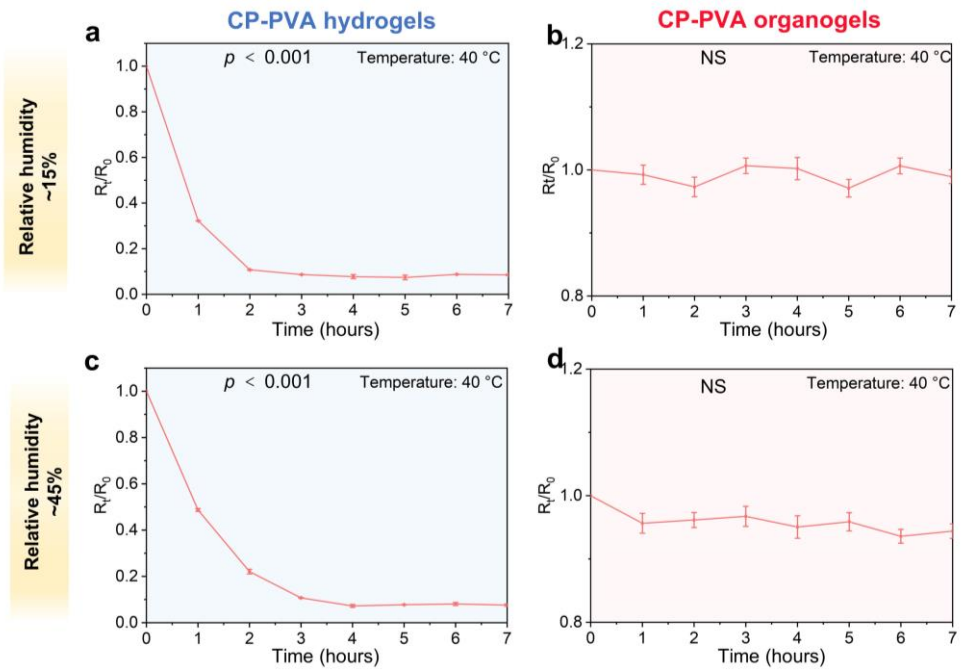

Supplementary Fig. 12 | Resistance changes of CP-PVA hydrogels and CP-PVA organogels at 40 °C. **a-d,** Resistance changes (R_t/R_0) of CP-PVA hydrogels (**a, c**) and CP-PVA organogels (**b, d**) when subject to environments with low (**a, b**) and high humidity (**c, d**) at 40 °C, where R_t refers to the resistance of the gels at different times and R_0 refers to the initial resistance of the gels. The CP-PVA organogels, with a solid content of ~50 wt% and CP's relative content of 22 wt%, were used for experiments. The hydrogel counterparts were prepared by dialyzing the corresponding organogels in water, followed by drying at the ambient environment (30 °C) and reswelling in purified water. The data in panel **a-d** are presented as mean values ± standard deviation (s.d.), with four samples tested in independent measurements. Statistical significance was assessed using ANOVA for comparisons among multiple groups (panel **a-d**), with significance levels denoted as $p \geq 0.05$ (not significant, NS), $p < 0.05$(*), $p < 0.01$(**), and $p < 0.001$(***).

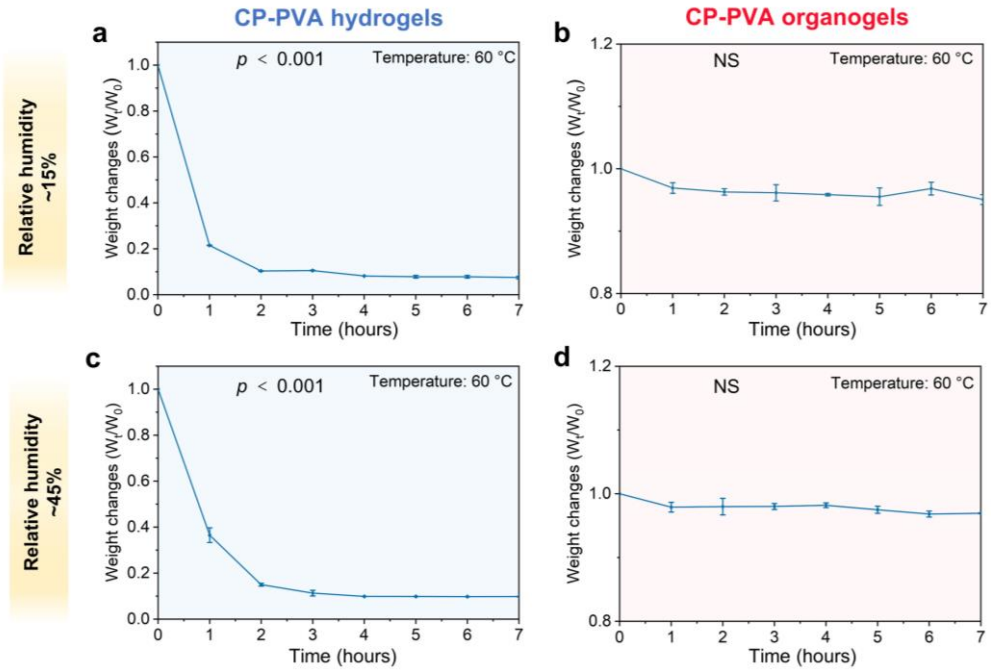

Supplementary Fig. 13 | Weight changes of CP-PVA hydrogels and CP-PVA organogels at 60 °C. a-d, Weight changes (W_t/W_0) of CP-PVA hydrogels (**a, c**) and CP-PVA organogels (**b, d**) when subject to environments with low (**a, b**) and high humidity (**c, d**) at 60 °C. The CP-PVA organogels, with a solid content of ~50 wt% and CP's relative content of 22 wt%, were used for experiments. The hydrogel counterparts were prepared by dialyzing the corresponding organogels in water, followed by drying at the ambient environment (25 ℃) and reswelling in purified water. Where W_t refers to the weights of the gels at different times, and W_0 refers to the initial weights of the gels. The data in (**a-d**) are presented as mean values ± standard deviation (s.d.), with four samples tested in independent measurements. Statistical significance was assessed using ANOVA for comparisons among multiple groups (panels **a-d**), with significance levels denoted as $p \geq 0.05$ (not significant, NS), $p < 0.05$(*), $p < 0.01$(**), and $p < 0.001$(***).

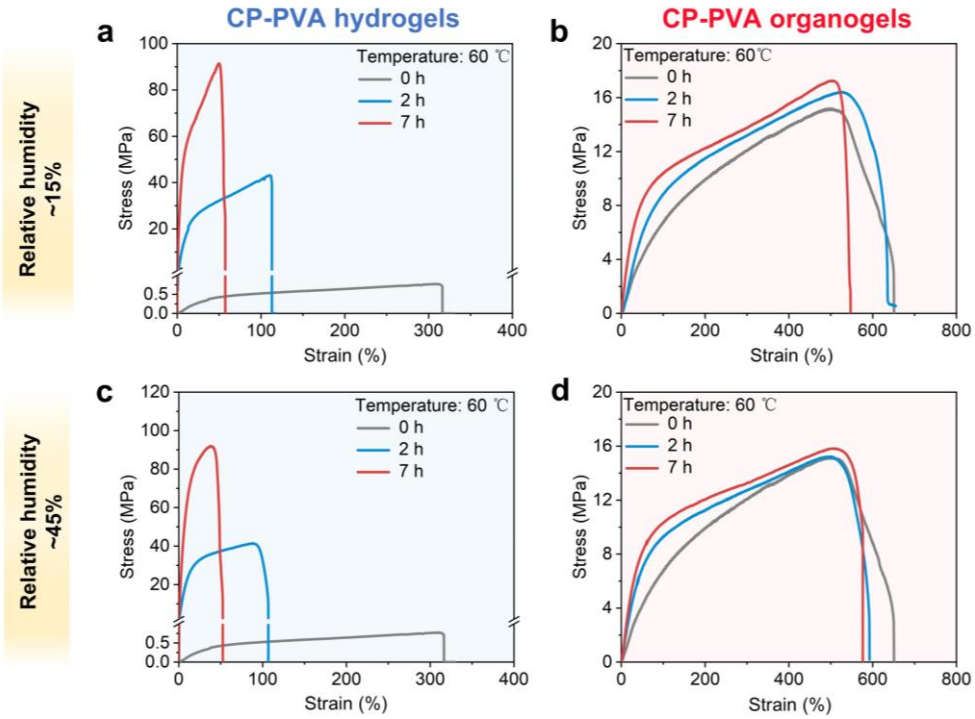

Supplementary Fig. 14 | The mechanical stability of CP-PVA hydrogels and CP-PVA organogels at 60 °C. a-d, Tensile stress-strain curves of CP-PVA hydrogels (**a, c**) and CP-PVA organogels (**b, d**) after being subjected to environments with low (**a, b**) and high humidity (**c, d**) at 60 °C for 7 hours. The stress-strain curves were recorded at a strain rate of 200% min^{-1}. The CP-PVA organogels, with a solid content of ~50 wt% and CP's relative content of 22 wt%, were used for experiments. The hydrogel counterparts were prepared by dialyzing the corresponding organogels in water, followed by drying at the ambient environment (25°C) and reswelling in purified water.

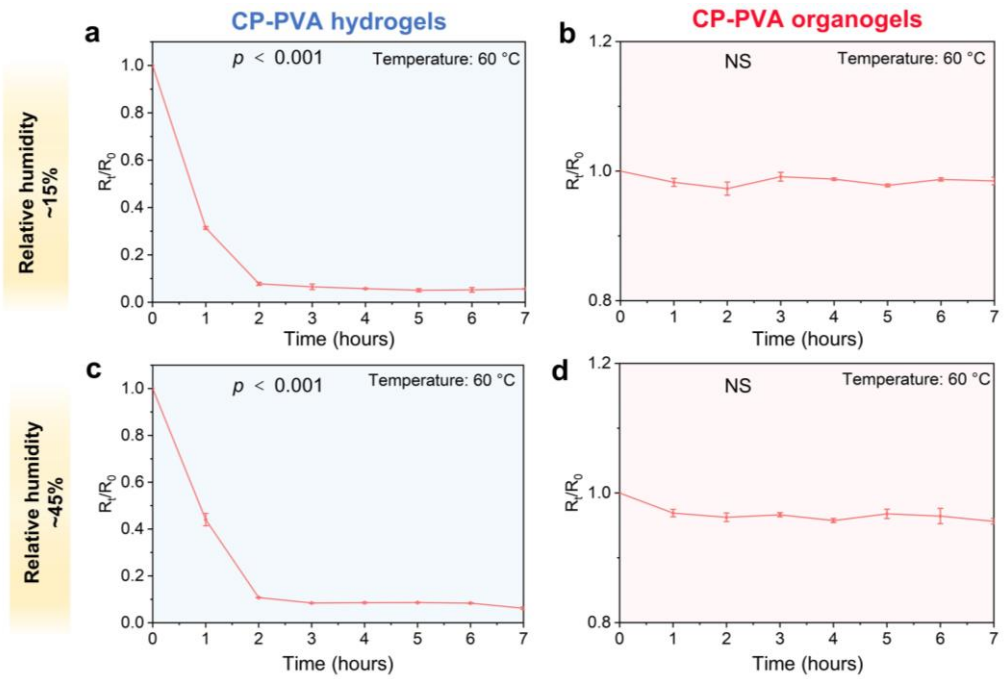

Supplementary Fig. 15 | Resistance changes of CP-PVA hydrogels and CP-PVA organogels at 60 °C. **a-d,** Resistance changes (R_t/R_0) of CP-PVA hydrogels (**a, c**) and CP-PVA organogels (**b, d**) when subject to environments with low (**a, b**) and high humidity (**c, d**) at 60 °C. The CP-PVA organogels, with a solid content of ~50 wt% and CP's relative content of 22 wt%, were used for experiments. The hydrogel counterparts were prepared by dialyzing the corresponding organogels in water, followed by drying at an ambient environment (25 °C) and reswelling in purified water. Where R_t refers to the resistance of the gels at different times, and R_0 refers to the initial resistance of the gels. The data in (**a-d**) are presented as mean values ±standard deviation (s.d.), with four samples tested in independent measurements. Statistical significance was assessed using ANOVA for comparisons among multiple groups (panels **a-d**), with significance levels denoted as $p \geq 0.05$ (not significant, NS), $p < 0.05$(*), $p < 0.01$(**), and $p < 0.001$(***).

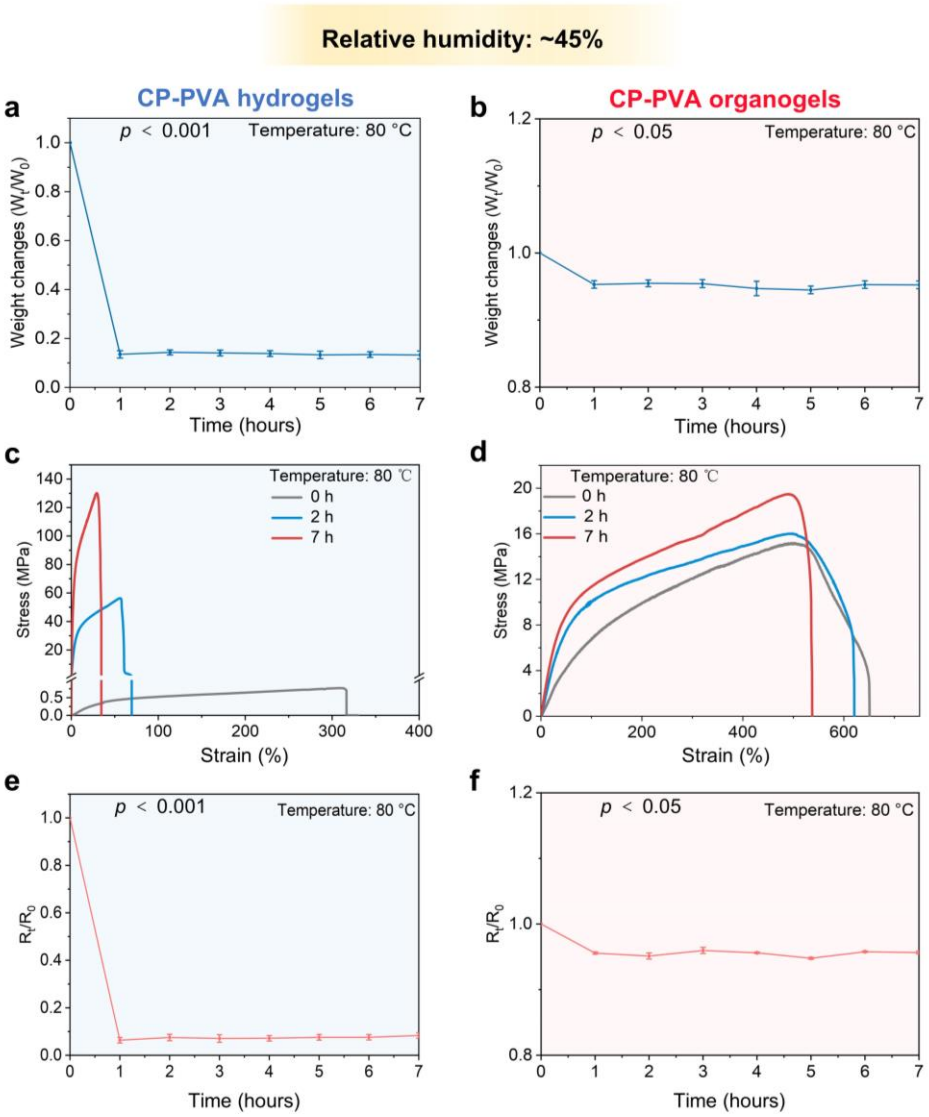

Supplementary Fig. 16 | Stability of CP-PVA hydrogels and CP-PVA organogels at 80 °C. a-f, Weight changes (W_t/W_0) (**a, b**), mechanical properties (**c, d**), and resistance change (R_t/R_0) (**e, f**) of CP-PVA hydrogels (**a, c,** and **e**) and CP-PVA organogels (**b, d,** and **f**) after subject to environments with a humidity of 45% at 80 °C for different times. The CP-PVA organogels, with a solid content of ~50 wt% and CP's relative content of 22 wt%, were used for experiments. The hydrogel counterparts were prepared by dialyzing the corresponding organogels in water, followed by drying at the ambient environment (25 °C) and reswelling in purified water. Where W_t refers to the weights of the gels at different times, W_0 refers to the initial weights of the gels, R_t refers to the resistance of the gels at different times, and R_0 refers to the initial resistance of the gels. The stress-strain curves in **c** and **d** were recorded at a strain rate of 200% min^{-1}. The data in (**a, b, e,** and **f**) are presented as mean values ± standard deviation (s.d.), with four samples tested in independent measurements. Statistical significance was assessed using ANOVA for comparisons among multiple groups (panel **a**, **b**, **e**, and **f**), with significance levels denoted as $p \geq 0.05$ (not significant, NS), $p < 0.05$(*), $p < 0.01$(**), and $p < 0.001$(***).

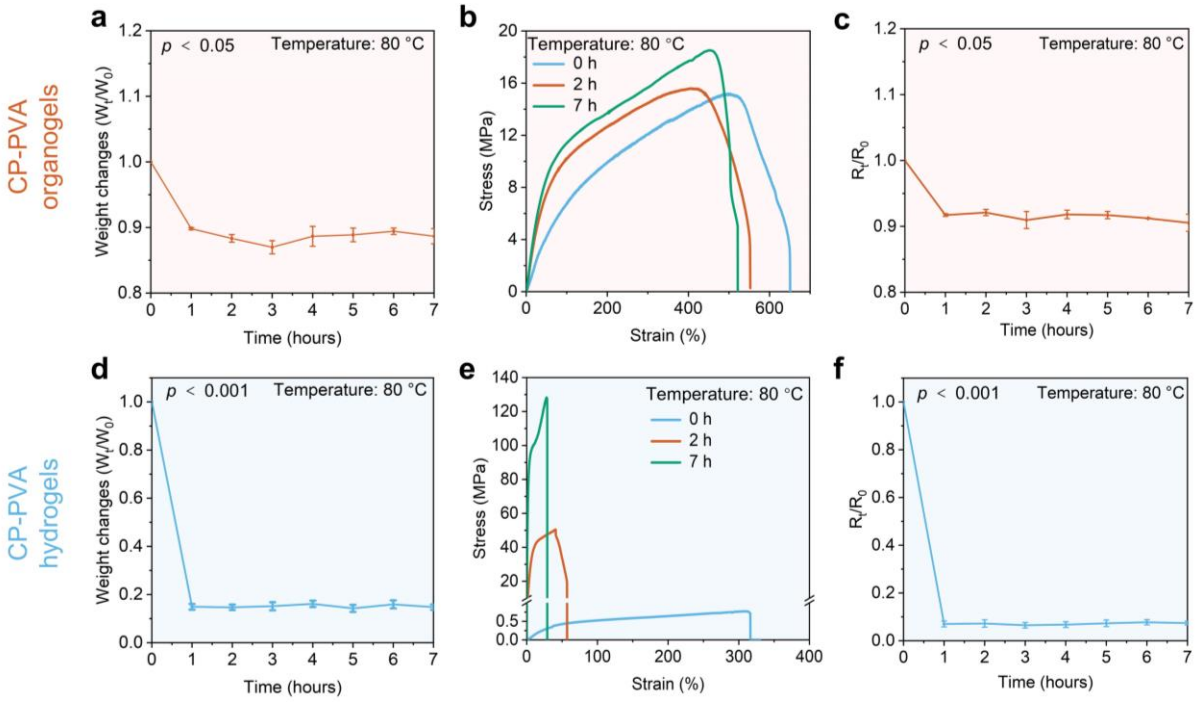

Supplementary Fig. 17 | Stability of CP-PVA hydrogels and CP-PVA organogels at 80 °C and 15% relative humidity. a-f, Weight changes (W_t/W_0) (**a, d**), mechanical properties (**b, e**), and resistance change (R_t/R_0) (**c, f**) of CP-PVA organogels (**a-c**) and CP-PVA hydrogels (**d-f**) after subject to environments with a humidity of 45% at 80 °C for different times. Where W_t refers to the weights of the gels at different times, W_0 refers to the initial weights of the gels, R_t refers to the resistance of the gels at different times, and R_0 refers to the initial resistance of the gels. The CP-PVA organogels, with a solid content of ~50 wt% and CP's relative content of 22 wt%, were used for experiments. The hydrogel counterparts were prepared by dialyzing the corresponding organogels in water, followed by drying at the ambient environment (25 °C) and reswelling in purified water. The stress-strain curves in panels **b** and **e** were recorded at a strain rate of 200% min^{-1}. The data in panels **a**, **c**, **d**, and **f** were presented as mean values ± standard deviation (s.d.), with four different samples examined in independent measurements. Statistical significances were assessed using one-way analysis of variance (ANOVA) for comparisons among multiple groups (panels **a**, **c**, **d**, and **f)**, with significance levels denoted as $p \geq 0.05$ (not significant, NS), $p < 0.05$(*), $p < 0.01$(**), and $p < 0.001$(***).

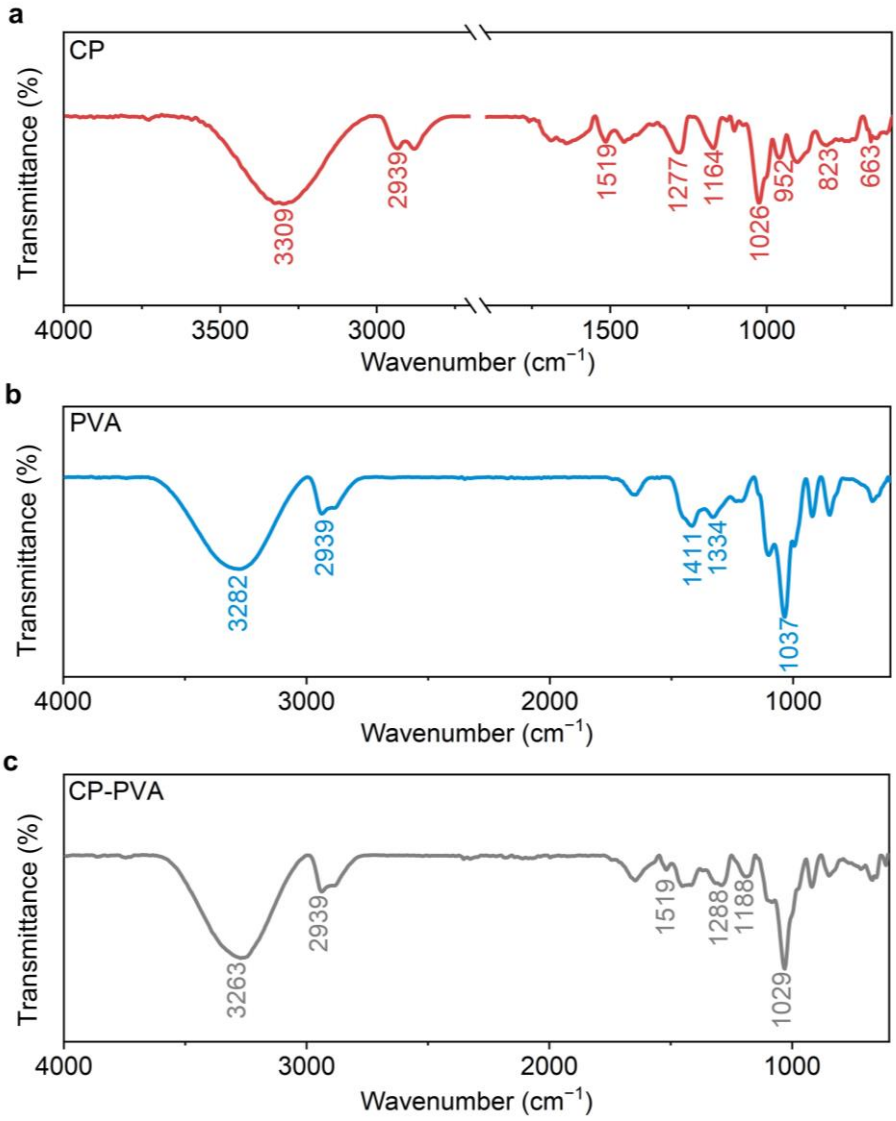

Supplementary Fig. 18 | Attenuated total reflectance Fourier-transform infrared (FT-IR) spectra of CP, PVA and CP-PVA organogels. a-c, The CP (**a**), PVA (**b**), and CP-PVA (**c**) organogels were directly used for the infrared spectroscopy tests. FT-IR spectra were recorded over the wavelength range of 700–4000 cm^{-1}, with scan numbers of 16 and a resolution of 4 cm^{-1}. The CP-PVA organogels with a CP's relative content of 22 wt% were used for tests. The detailed band assignments are listed in Supplementary Tables 2, 3, and 4.

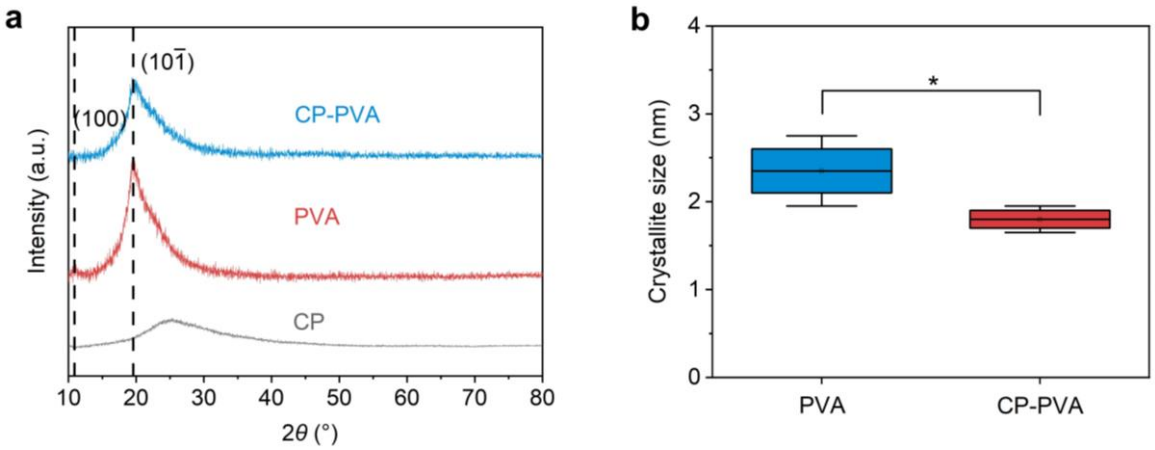

Supplementary Fig. 19 | X-ray diffraction (XRD) characterization of CP, PVA, and CP-PVA organogels. **a,** XRD patterns of CP, PVA, and CP-PVA organogels. The CP-PVA organogels used had a solid content of ~50 wt% with CP's relative content of 22 wt%. The diffraction peaks at 11.5° and 19.5° were ascribed to the (100) and (10$\bar{1}$) crystalline faces of PVA, respectively. **b,** Comparisons on the average crystallite size of PVA organogels before and after CP were introduced, calculated from the full-width at half-maximum (FWHM) for the peak at 19.5°. The data in panel **b** are presented as mean ± standard deviation (s.d.) from four independent samples. The data in panel **b** are presented in box-and-whisker plots, where the central dots, lines, and box limits indicate the mean, the median, and the upper/lower quartiles, and the whiskers extend to 1.5× the interquartile range from the quartiles. Statistical significance was assessed using two-sided *t*-tests for comparisons between two groups (panels **b**), with significance levels denoted as $p \geq 0.05$ (not significant, NS), $p < 0.05$(*), $p < 0.01$(**), and $p < 0.001$(***).

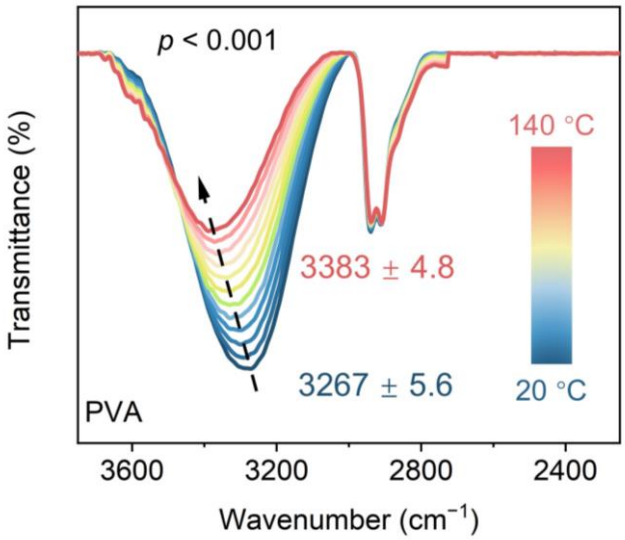

Supplementary Fig. 20 | Temperature-dependent FT-IR spectra of pure PVA organogels. The pure PVA organogels were prepared through a procedure similar to that of CP-PVA organogels as described in the experimental section, except that the glycerol solutions with 100 mg mL^{-1} of PVA (glycerol's content: 4 wt%, relative to the total mass of suspension) were utilized as precursor solution at the beginning of preparation. The PVA organogels were directly used for the tests. FT-IR spectra were recorded over the wavelength range of 2200–3800 cm^{-1}, with scan numbers of 16 and a resolution of 4 cm^{-1}. The temperature was controlled in a range of 20-140 °C with an interval of 10 °C. The peak at ~3200 cm^{-1} ascribed to hydroxyl groups (from PVA and glycerol) shifted to a higher wavenumber as the temperature increased from 20 °C to 140 °C. This blue shift indicated the dissociation of hydrogen bonds at elevated temperatures, suggesting a reduction in the crosslinking density of the polymer networks. It is worth noting that the organogels remained stable with a low degree of dehydration during the test, given the measurement at each temperature took only a short time of ~2 minutes. The data are presented as mean ± standard deviation (s.d.) from four independent samples. Statistical significance was assessed using ANOVA for comparisons among multiple groups, with significance levels denoted as $p \geq 0.05$ (not significant, NS), $p < 0.05$(*), $p < 0.01$(**), and $p < 0.001$(***).

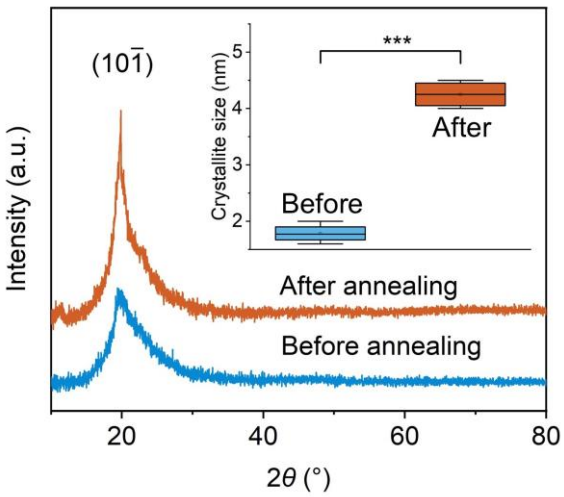

Supplementary Fig. 21 | X-ray diffraction (XRD) characterization of CP-PVA organogels before and after annealing. Representative XRD profiles of CP-PVA organogels before and after thermal annealing at 80 °C for 2 hours. The unannealed p-CP-PVA organogels used for the tests had a solid content of ~40 wt% with CP's relative content of 22 wt% (relative to the total mass of CP and PVA). The diffraction peaks at 19.5° were ascribed to (10$\bar{1}$) crystalline facets of PVA chains in the CP-PVA hydrogels. The insets depict the average crystallite size change of CP-PVA organogels after thermal annealing, calculated from the FWHM for the peak at 19.5°. The data in the panel inset are presented as mean values ± standard deviation (s.d.), with four samples tested in independent measurements. The data in the inset are presented in box-and-whisker plots, where the central dots, lines, and box limits indicate the mean, the median, and the upper/lower quartiles, and the whiskers extend to 1.5× the interquartile range from the quartiles. Statistical significance was assessed using two-sided *t*-tests for comparisons between two groups (inset), with significance levels denoted as $p \geq 0.05$ (not significant, NS), $p < 0.05$(*), $p < 0.01$(**), and $p < 0.001$(***).

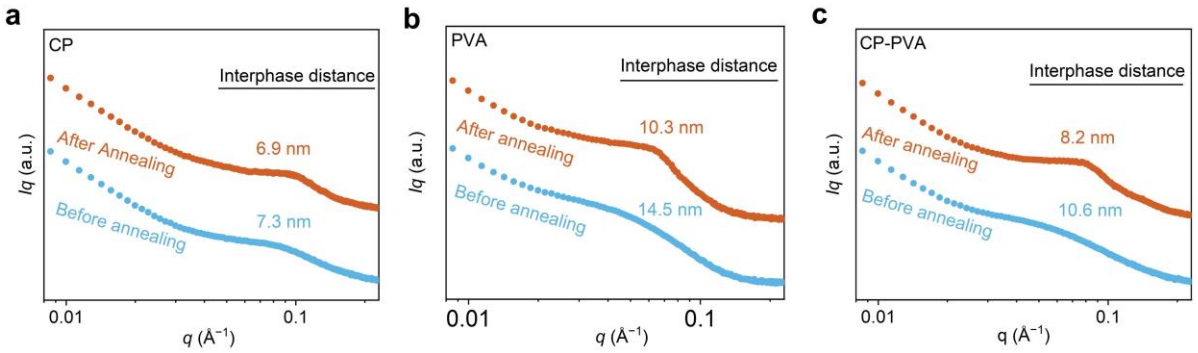

Supplementary Fig. 22 | SAXS profiles of CP, PVA, and CP-PVA organogels. a, Pure CP organogels; **b,** pure PVA organogels; **c,** pure CP organogels. The pure PVA and CP organogels were prepared through a procedure similar to that of CP-PVA organogels as described in the experimental section, except that the glycerol solutions with 26.1 mg mL^{-1} of PVA or 7.4 mg mL^{-1} of CP (glycerol content: 4 wt% relative to the total mass of suspension) were utilized as precursor solution at the beginning of preparation. When compared to before annealing, the scattering peak of CP-PVA organogels after annealing strengthened with a positive shift (corresponding to the decrease in the average interphase distance), similar to the trend observed for the pure PVA and pure CP organogels. Such transformation indicated the thermal treatment induced the partial perfection of PVA and PEDOT crystalline domains.

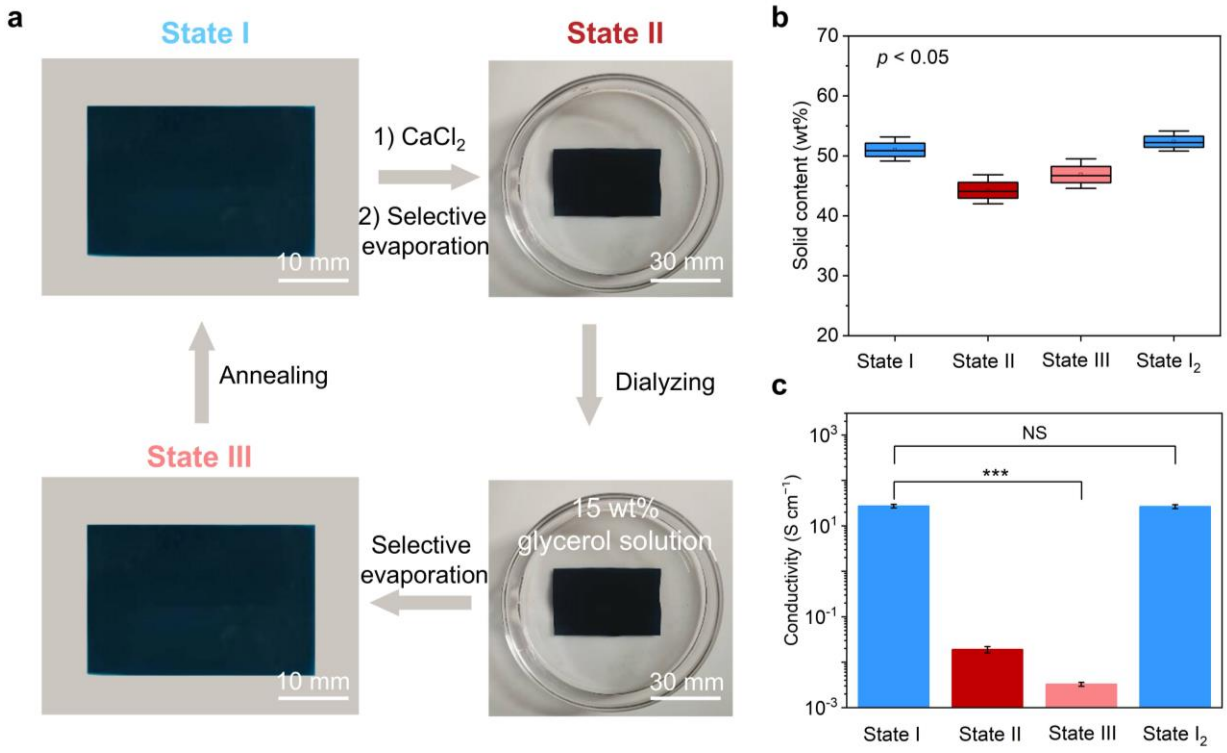

Supplementary Fig. 23 | Photographs, solid contents, and conductivities of CP-PVA organogel at different states. a, Digital photographs of CP-PVA organogels at different states. The CP-PVA organogels used for the tests had a solid content of ~50 wt% with CP's relative content of 22 wt%. The CP-PVA organogels maintained excellent structural integrity upon the chemical and physical treatments. **b-c,** The solid contents (**b**) and conductivity (**c**) of CP-PVA organogels at different states. For the preparation of CP-PVA organogels at State II, the thermally-annealed CP-PVA organogels (State I) (CP's relative content: 22 wt%, solid content: ~50 wt%) were soaked with a glycerol solution containing 2 mol L^{-1} Ca^{2+} ion for 3 days, followed by selective evaporation at an ambient environment for 24 hours. For the preparation of CP-PVA organogels at State III, the CP-PVA organogels at State II were dialyzed in a 15 wt% of glycerol solution for 24 hours and partially dried at an ambient environment for 24 hours to evaporate most of the water. At last, the CP-PVA organogel at State III could be transformed back to State I (denoted as State I_2) through thermal annealing at 80 °C for 2 hours. The data in panels **b** and **c** are presented as mean values ± standard deviation (s.d.), with four samples tested in independent measurements. The data in panel **b** are presented in box-and-whisker plots, where the central dots, lines, and box limits indicate the mean, the median, and the upper/lower quartiles, and the whiskers extend to 1.5× the interquartile range from the quartiles. Statistical significance was assessed using one-way analysis of variance (ANOVA) for comparisons among multiple groups (panels **b**) and two-sided t-tests for comparisons between two groups (panel **c**), with significance levels denoted as $p \geq 0.05$ (not significant, NS), $p < 0.05$(*), $p < 0.01$(**), and $p < 0.001$(***).

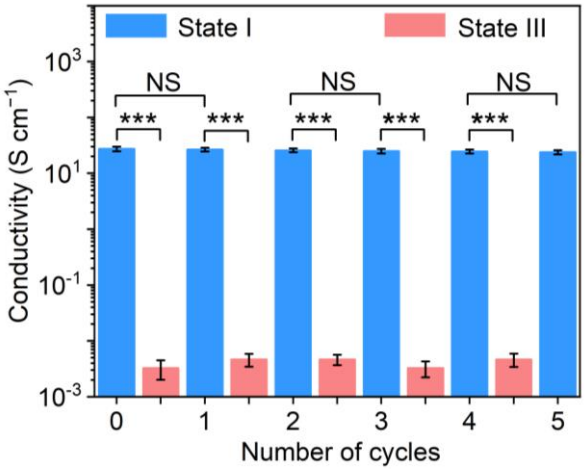

Supplementary Fig. 24 | Cyclic stability of CP-PVA organogels during switching between State I and State III. The CP-PVA organogels (CP's relative content: 22 wt%, solid content: ~50 wt%) demonstrated reversible switching between a high-conductance state (State I) and a high-resistance state (State III) via the treating procedure outlined in the Supplementary Fig. 23. This switching process could be repeated over 5 times with no significant alteration in the electrical performance. The data are presented as mean values ± standard deviation (s.d.), with four different samples examined in independent measurements. Statistical significance was assessed using two-sided *t*-tests for comparisons between two groups, with significance levels denoted as $p \geq 0.05$ (not significant, NS), $p < 0.05$(*), $p < 0.01$(**), and $p < 0.001$(***).

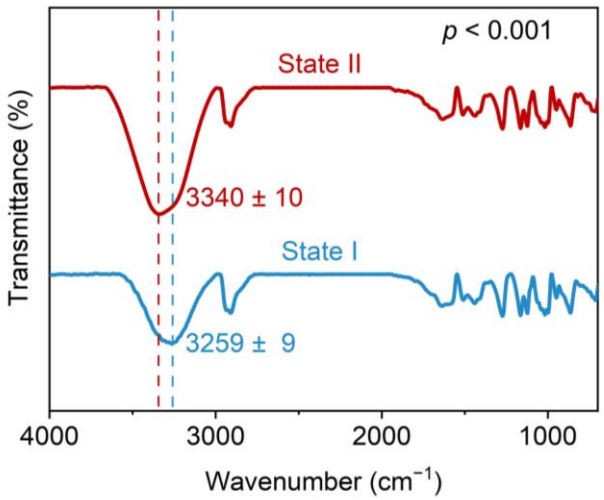

Supplementary Fig. 25 | FT-IR spectra of PVA-CP organogels at States I and II. The characteristic hydroxy-related peak shifted from 3259 cm^{-1} to 3340 cm^{-1} when the organogels were transitioned from State I to State II, indicating the dissociation of hydrogen bonds within the CP-PVA organogels after the $CaCl_2$ treatment. The CP-PVA organogels used for the tests had a solid content of ~50 wt% with CP's relative content of 22 wt%. The FT-IR spectra were recorded with scan numbers of 16 and a resolution of 4 cm^{-1}. The data are presented as mean values ± standard deviation (s.d.), with four different samples examined in independent measurements. Statistical significance was assessed using two-sided *t*-tests for comparisons between two groups, with significance levels denoted as $p \geq 0.05$ (not significant, NS), $p < 0.05$(*), $p < 0.01$(**), and $p < 0.001$(***).

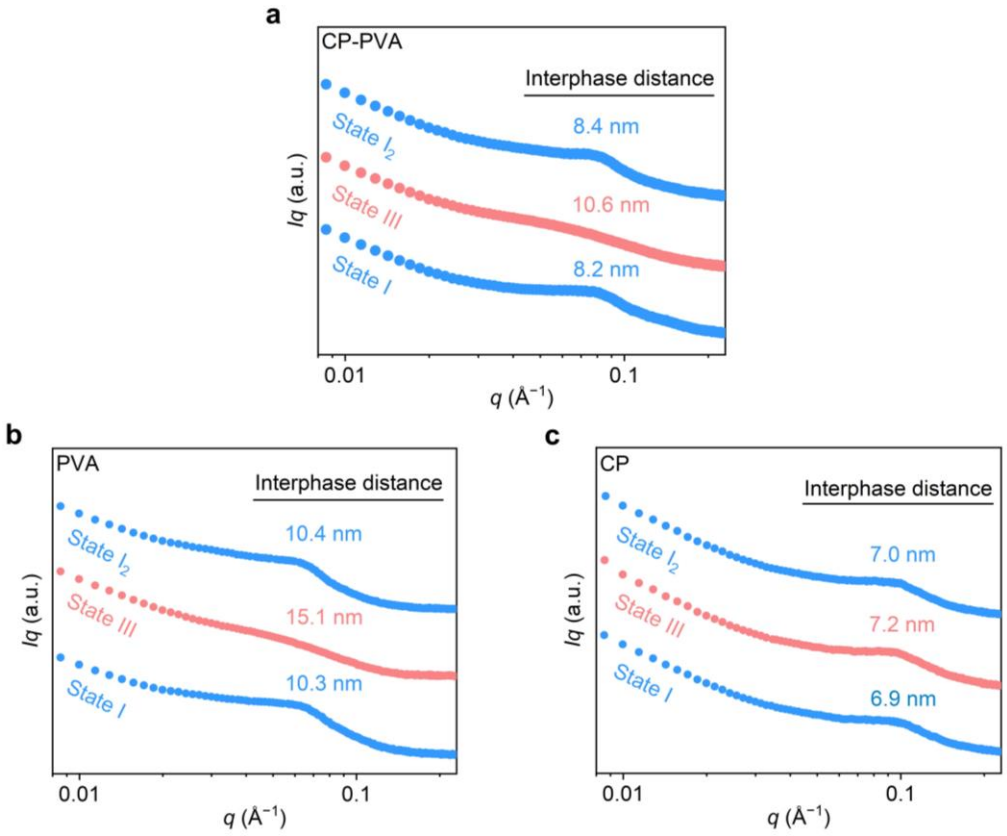

Supplementary Fig. 26 | Small-angle X-ray scattering (SAXS) profiles of CP-PVA, PVA and CP organogels at different states. a, CP-PVA organogels; **b,** pure PVA organogels; **c,** pure CP organogels. The pure PVA and CP organogels were prepared through a procedure similar to that of CP-PVA organogels as described in the experimental section, except that the glycerol solutions with 100 mg mL^{-1} of PVA or 7.4 mg mL^{-1} of CP (glycerol's content: 4 wt%, relative to the total mass of suspension) were utilized as precursor solution at the beginning of preparation. When compared to that in State I, the scattering peak of CP-PVA organogels in State III weakened with a negative shift (corresponding to the increase in average interphase distance), similar to the trend observed for the pure PVA organogels. Such transformation indicated the $CaCl_2$ treatment induced the partial disassociation of PVA crystalline domains. In comparison, the pure CP organogels remained nearly intact toward $CaCl_2$ treatment, revealing the high dynamics of CP-PVA organogels mainly originated from PVA chains. Additionally, the regulation of phase structure was reversible, as revealed by the recovery of the SAXS spectra of CP-PVA and PVA organogels through dialysis and thermal annealing (denoted as State I_2).

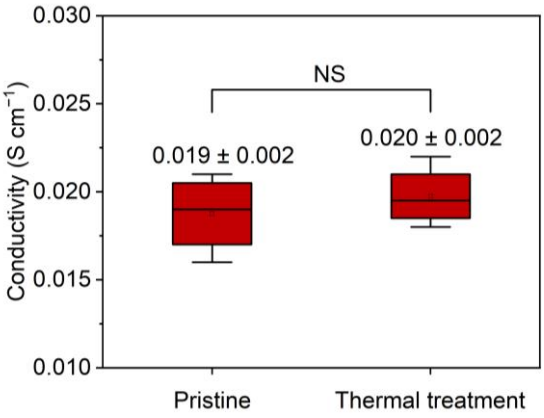

Supplementary Fig. 27 | Thermodynamic stability of CP-PVA organogel in State II. The conductivity of CP-PVA organogels in State II before and after thermal treatment at 60 °C for 5 hours in 15 wt% of glycerol solution containing 2 mol L^{-1} of $CaCl_2$ (followed by selective evaporation at the ambient environment for 24 hours to evaporate most of the water). The conductivities were measured using a four-point probe method with a digital source meter. The data are presented as mean values ± standard deviation (s.d.), with four different samples examined in independent measurements. The data are presented in box-and-whisker plots, where the central dots, lines, and box limits indicate the mean, the median, and the upper/lower quartiles, and the whiskers extend to 1.5× the interquartile range from the quartiles. Statistical significance was assessed using two-sided *t*-tests for comparisons between two groups, with significance levels denoted as $p \geq 0.05$ (not significant, NS), $p < 0.05$(*), $p < 0.01$(**), and $p < 0.001$(***).

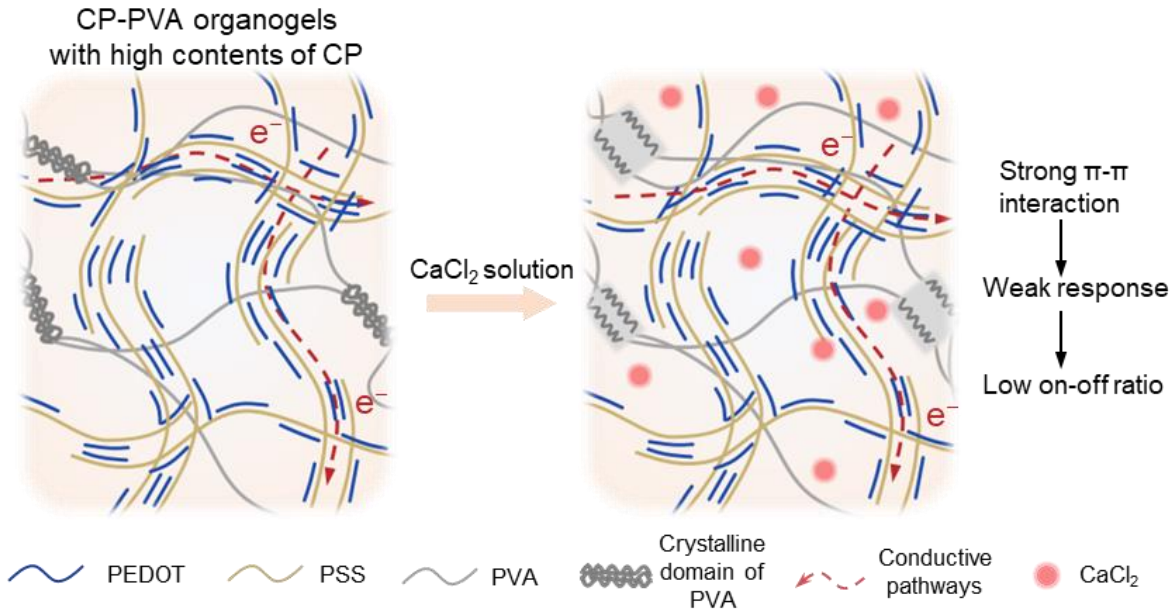

Supplementary Fig. 28 | Schematic illustration of the effect of varying PVA content on the on-off ratio of PVA-CP organogels. Decreasing the relative content of PVA improved the overall conductivity but reduced the on-off ratio, likely due to the reduced polymer chain dynamics and the dominance of π-π interactions from PEDOT chains as PVA content decreased.

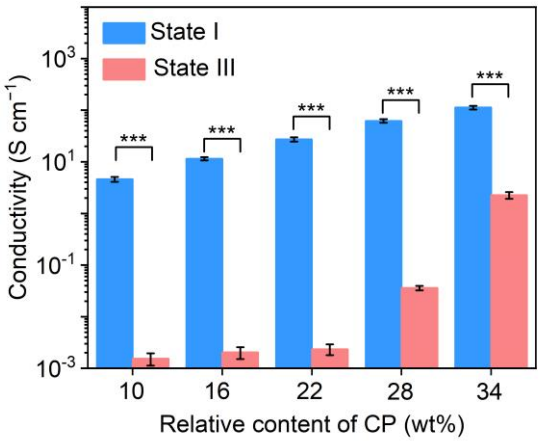

Supplementary Fig. 29 | Conductance regulation of CP-PVA organogels with different relative contents of CP. CP-PVA organogels with a low relative content of CP (corresponding to a high relative content of PVA) exhibited relatively low conductivity but showed a high tunability of conductance. This could be explained by the decreased dynamics of the composite networks with the relative content of the component (PVA) decreasing, where PEDOT chains with weak responses to specific ion effects gradually dominated and stabilized the overall conductive networks. The data are presented as mean values ± standard deviation (s.d.), with four different samples examined in independent measurements. Statistical significance was assessed using two-sided *t*-tests for comparisons between two groups, with significance levels denoted as $p \geq 0.05$ (not significant, NS), $p < 0.05$(*), $p < 0.01$(**), and $p < 0.001$(***).

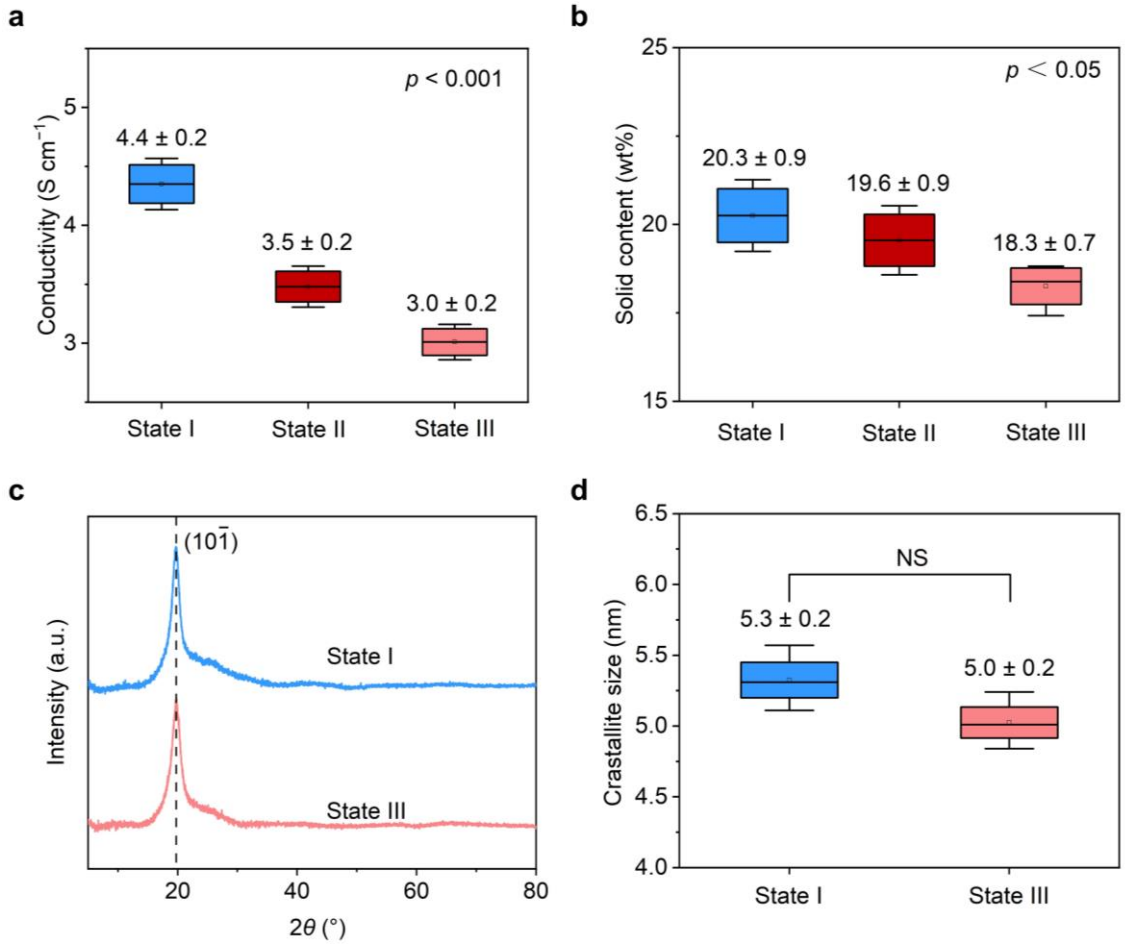

Supplementary Fig. 30 | Conductivities, solid contents, and XRD characterizations of CP-PVA hydrogels at State I and III. The CP-PVA hydrogel (State I) was prepared by a drying-reswelling method, where a 4 wt% of glycerol solution containing CP and PVA (CP's relative content: 22 wt%) was drop-casted onto a glass substrate, thermally annealed at 80 °C for 2 hours followed by dialyzing the organogels in water, followed by drying at the ambient environment (25 °C) and reswelling in purified water. Subsequently, the resulting CP-PVA hydrogel (State I) was treated with $CaCl_2$ solution and then dialyzed in purified water for 24 hours to obtain the hydrogel at State III. **a, b,** The conductivity (**a**) and solid contents (**b**) of CP-PVA organogels at different states. The CP-PVA hydrogel at State II showed similar conductivity to that of hydrogel at State I, indicating the weak response of the CP-PVA hydrogel system toward $CaCl_2$ treatment. The weak response was probably due to the restriction of PVA chain motion by PEDOT:PSS chains, especially in the absence of glycerol serving as an efficient plasticizer. **c, d,** XRD patterns of CP-PVA hydrogels. The diffraction peaks at 19.5° were ascribed to (10$\bar{1}$) crystalline facets of PVA chains in the CP-PVA hydrogels. The average crystalline sizes of CP-PVA hydrogels were calculated from the full-width at half-maximum (FWHM) for the peak at 19.5°. The data in panels **a**, **b**, and **d** are presented as mean values ± standard deviation (s.d.), with four different samples examined in independent measurements. The data in panels **a**, **b,** and **d** are presented in box-and-whisker plots, where the central dots, lines, and box limits indicate the mean, the median, and the upper/lower quartiles, and the whiskers extend to 1.5× the interquartile range from the quartiles. Statistical significance was assessed using two-sided *t*-tests for comparisons between two groups (panel **d**) and ANOVA for comparisons among multiple groups (panel **a** and **b**), with significance levels denoted as $p \geq 0.05$ (not significant, NS), $p < 0.05$(*), $p < 0.01$(**), and $p < 0.001$(***).

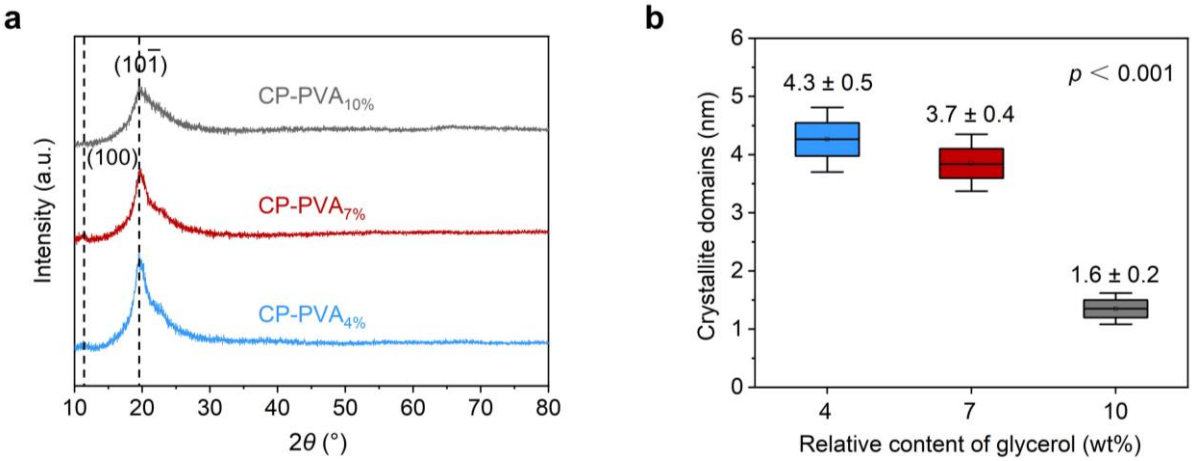

Supplementary Fig. 31 | X-ray diffraction (XRD) characterization of CP-PVA organogels with different contents of glycerol. a, XRD patterns of CP-PVA organogels with different relative contents of glycerol ranging from 4 wt% to 10 wt% (relative to the total mass of the precursor suspension used for preparation, denoted as CP-PVA$_{4\%}$, CP-PVA$_{7\%}$, CP-PVA$_{10\%}$). All the tested CP-PVA organogels had a CP's relative content of 22 wt% (relative to the total mass of the PVA and CP). The diffraction peaks at 11.5° and 19.5° were ascribed to the (100) and (10$\bar{1}$) crystalline faces of PVA, respectively. **b,** Comparisons on the average crystallite size of CP-PVA organogels with different relative contents of glycerol were introduced, calculated from the full-width at FWHM for the peak at 19.5°. The data in **b** are presented as mean values ± standard deviation (s.d.), with four samples tested in independent measurements. The data in panel **b** are presented in box-and-whisker plots, where the central dots, lines, and box limits indicate the mean, the median, and the upper/lower quartiles, and the whiskers extend to 1.5× the interquartile range from the quartiles. Statistical significance was assessed using ANOVA for comparisons among multiple groups (panel **b**), with significance levels denoted as $p \geq 0.05$ (not significant, NS), $p < 0.05$(*), $p < 0.01$(**), and $p < 0.001$(***).

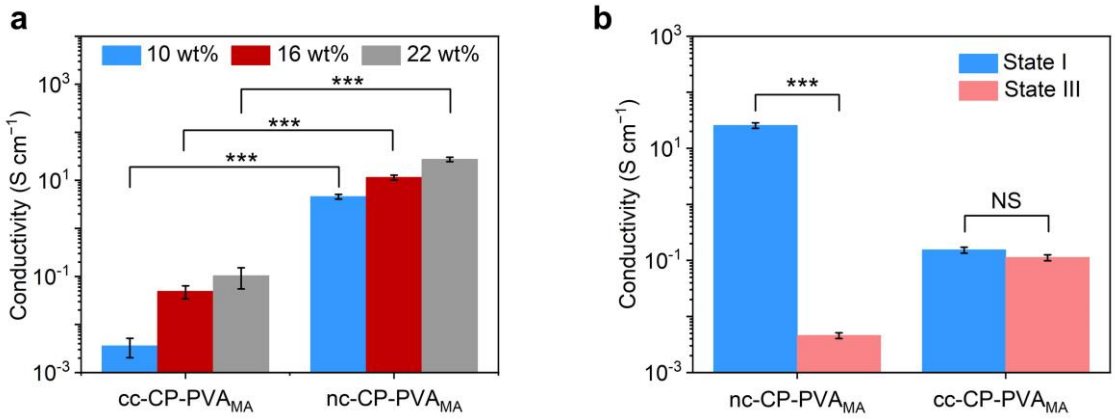

Supplementary Fig. 32 | Conductivity of CP-PVA$_{MA}$ organogels with or without chemical crosslinking. **a,** Conductivity of chemically-crosslinked or non-crosslinked CP-PVA$_{MA}$ organogels with varying CP contents (denoted as cc-CP-PVA$_{MA}$ and nc-CP-PVA$_{MA}$) after thermal treatment (no salt treatment). **b,** Conductivities of cc-CP-PVA$_{MA}$ and nc-CP-PVA$_{MA}$ with a CP's content of 22 wt% (relative to the total mass of CP and PVA$_{MA}$) before (State I) and after salt treatment (State III). The cc-CP-PVA$_{MA}$ organogels were prepared from CP and PVA$_{MA}$ through a similar procedure to that for CP-PVA organogels except that an ultraviolet (UV)-induced chemical crosslinking was implemented before thermal annealing (see detailed preparation in experimental section). For the nc-CP-PVA$_{MA}$, UV exposure was omitted and a polymerization inhibitor was added to the precursor solution (see detailed preparation procedure in the experimental section). The thermally-annealed nc-CP-PVA$_{MA}$ exhibited high conductivity and good conductance tunability, comparable to CP-PVA organogels, while the cc-CP-PVA$_{MA}$ organogels exhibited a one-order-of-magnitudes decrease in conductivity with a loss of conductance tunability. These results demonstrated that chain motion took an essential role in the reconfigurability of CP-PVA organogels. The data in panels **a**, **b** are presented as mean values ± standard deviation (s.d.), with four different samples examined in independent measurements. Statistical significance was assessed using two-sided *t*-tests for comparisons between two groups (panels **a** and **b**), with significance levels denoted as $p \geq 0.05$ (not significant, NS), $p < 0.05$(*), $p < 0.01$(**), and $p < 0.001$(***).

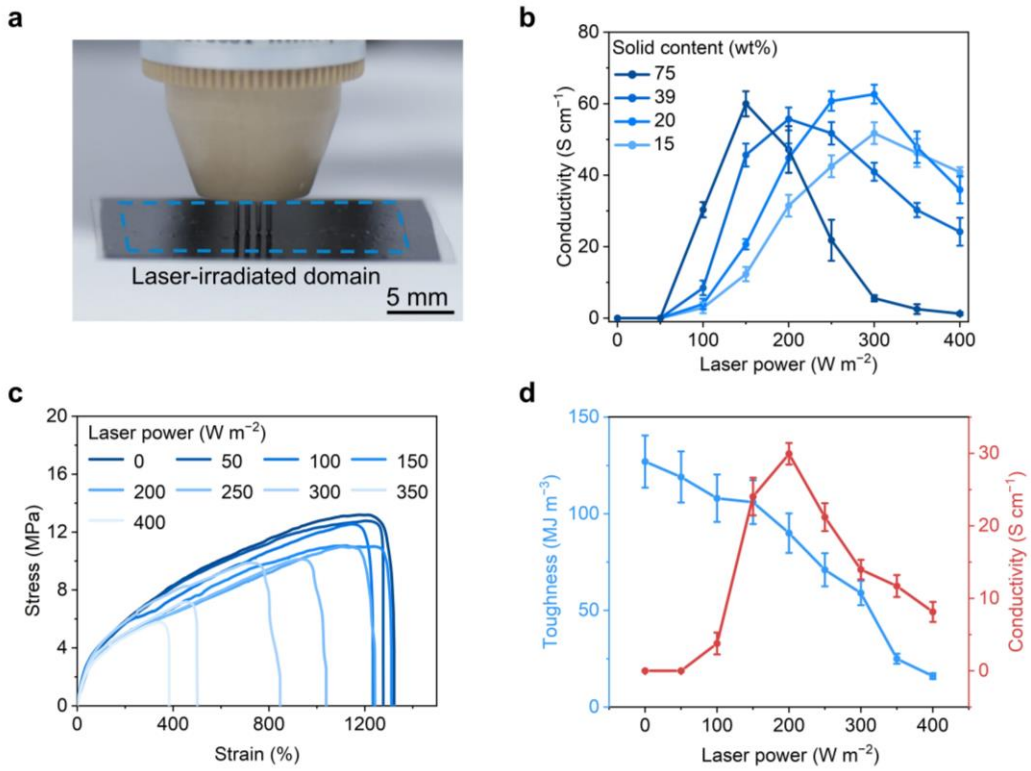

Supplementary Fig. 33 | The effect of laser power on the conductivity and mechanical properties of CP-PVA organogels. To trigger the transformation from low conductance states to high conductance states, CP-PVA organogels at State III (CP's relative content: 22 wt% relative to the total mass of CP and PVA) were exposed to laser irradiation (wavelength: 532 nm, diameter of laser spot: 0.3 mm) with laser power density ranging from 50 to 400 W m^{-2} at a fixed scanning speed of 6 cm s^{-1}. **a, b,** Digital photographs (**a**) and conductivities (**b**) of CP-PVA organogels with different solid contents after laser irradiation at different laser power, measured using a four-point probe method. **c,** Stress-strain curves of CP-PVA organogels after laser irradiation measured at a strain rate of 200% min^{-1}. **d,** Conductivity and toughness of CP-PVA organogels after laser-irradiated. The data in panels **b** and **d** were presented as mean values ± standard deviation (s.d.), with four different samples examined in independent measurements.

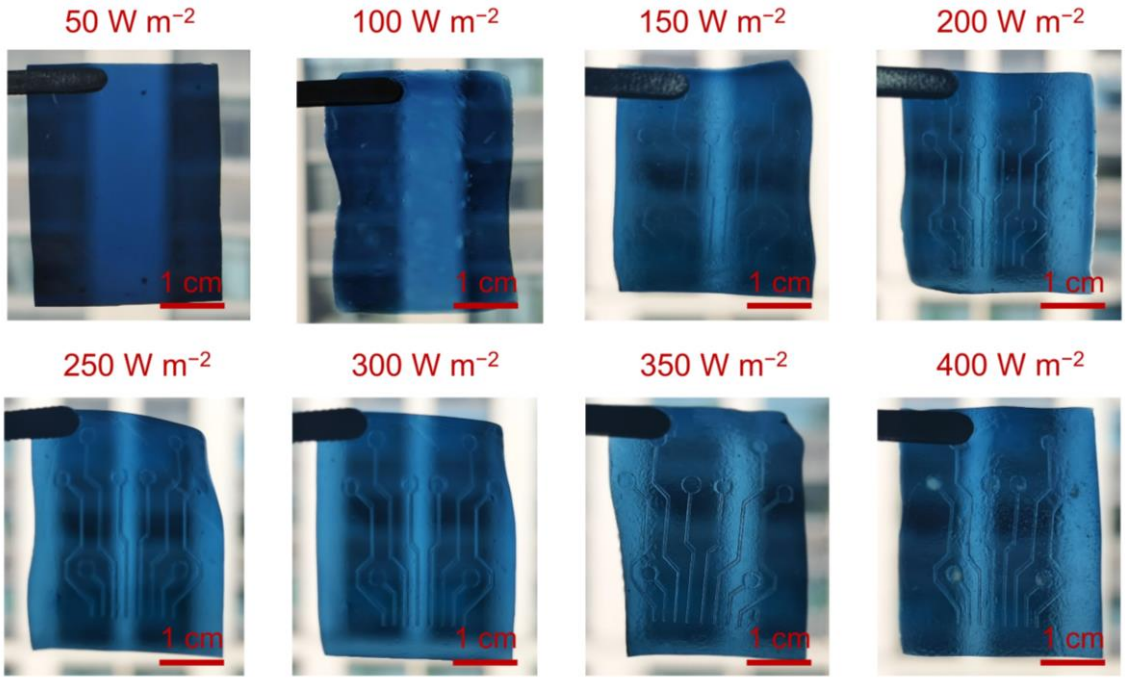

Supplementary Fig. 34 | Digital photographs of CP-PVA organogels with patterned conductive traces through laser-irradiated at different laser power. CP-PVA organogels at State III (solid contents: ~50 wt%, CP's relative content: 22 wt%) with a thickness of ~75 μm were irradiated with a continuous wave laser (wavelength: 532 nm, diameter of laser spot: 0.3 mm) at a fixed scanning speed of 6 cm s^{-1}, with power ranging from 50 to 400 W m^{-2}. At relatively low power (< 200 W m^{-2}), laser scanning has minimal impact on the geometric shape of CP-PVA organogels, with laser-scanned traces almost invisible to the naked eye. However, with the power density beyond 200 W m^{-2}, the laser-scanned trace became pronounced, indicating significant structural changes probably due to the evaporation of glycerol at high local temperatures (See temperature distribution in Supplementary Fig. 33).

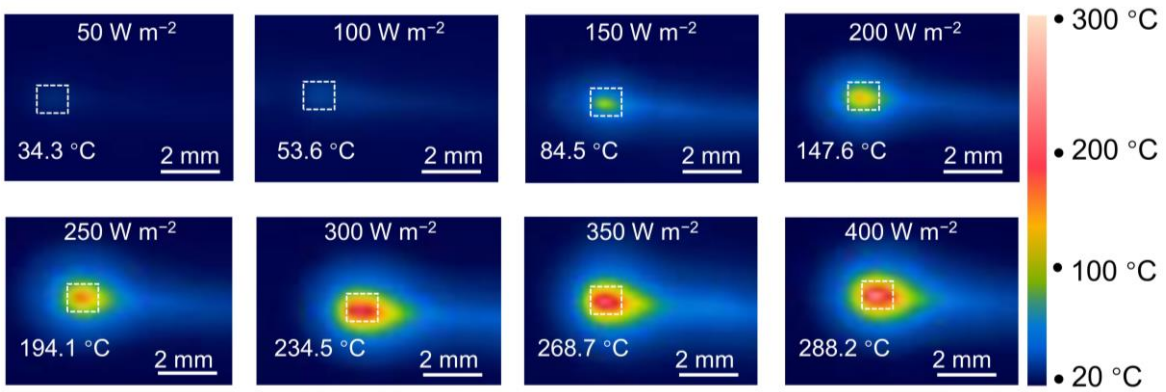

Supplementary Fig. 35 | Infrared thermography (IRT) of CP-PVA organogels under laser irradiation at different power. Infrared thermal images of CP-PVA organogels (solid contents: ~50 wt%, relative to the total mass of organogel, CP's content: 22 wt% relative to the total mass of CP and PVA, thickness: ~75 μm) irradiated at different power intensities (wavelength: 532 nm; diameter of laser spot: 0.3 mm; scanning speed: 6 cm s^{-1}) (bottom temperature: ~20 °C). The maximum temperatures reached during laser irradiation are indicated in the corresponding images.

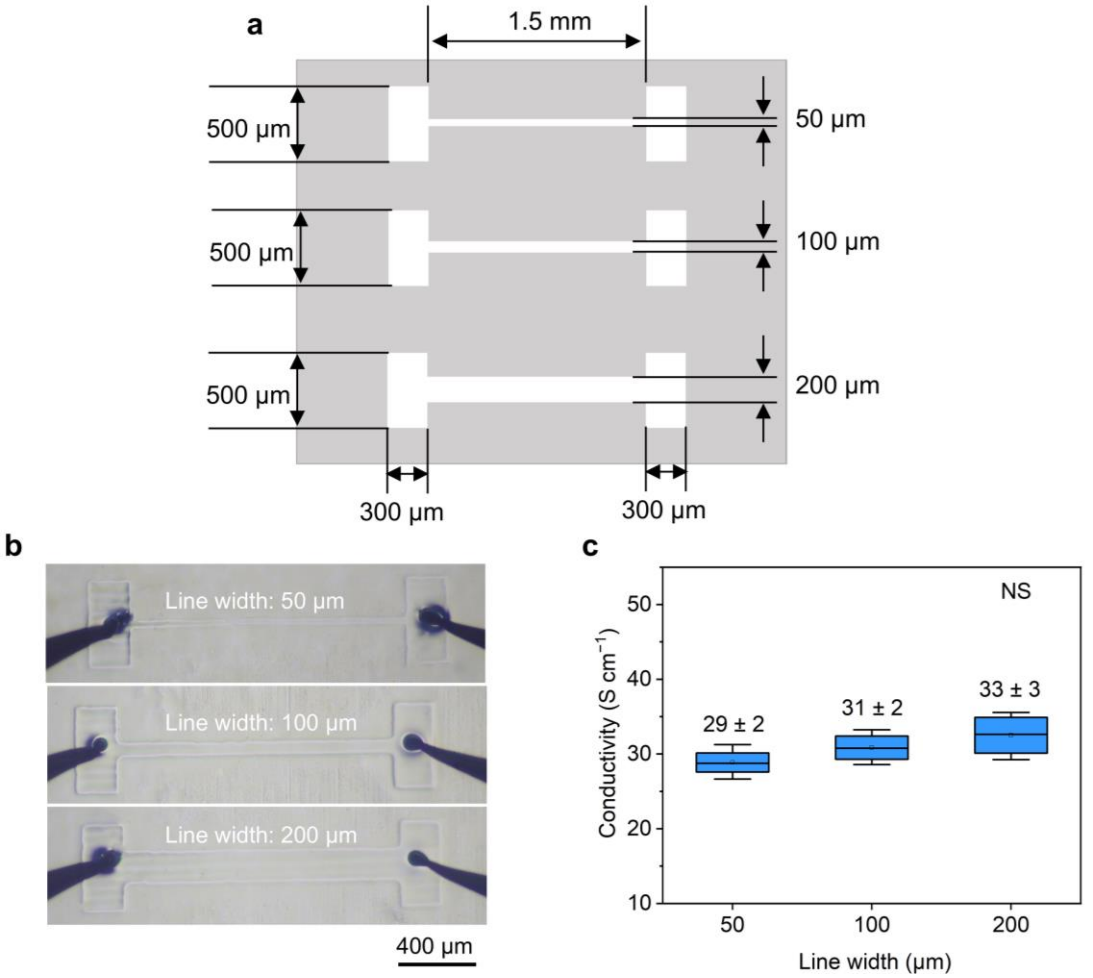

Supplementary Fig. 36 | Spatial resolution of laser-patterned conductive traces. CP-PVA organogels at State III (solid contents: ~50 wt%, relative to the total mass of organogel, CP's content: 22 wt% relative to the total mass of CP and PVA, thickness: ~75 μm) were irradiated with a continuous wave laser (wavelength: 532 nm; diameter of laser spot: 0.3 mm; power: 150 W m^{-2}) at a fixed scanning speed of 6 cm s^{-1} through a photomask. **a,** Schematic of the photomask used for circuit fabrication, where white and grey regions denote transparent and non-transparent areas, respectively. **b,** Microscopic images of CP-PVA organogels with patterned conductive traces. **c,** Conductivity of the patterned traces measured using a two-probe method. To minimize the contact resistance, probe tips were pre-coated with silver paste before tests. The data in panel **c** are presented as mean ± standard deviation (s.d.) from four independent samples. The data in panel **c** are presented in box-and-whisker plots, where the central dots, lines, and box limits indicate the mean, the median, and the upper/lower quartiles, and the whiskers extend to 1.5× the interquartile range from the quartiles. Statistical significance was assessed using one-way analysis of variance (ANOVA) for comparisons among multiple groups (panel **c**), with significance levels denoted as $p \geq 0.05$ (not significant, NS), $p < 0.05$(*), $p < 0.01$(**), and $p < 0.001$(***).

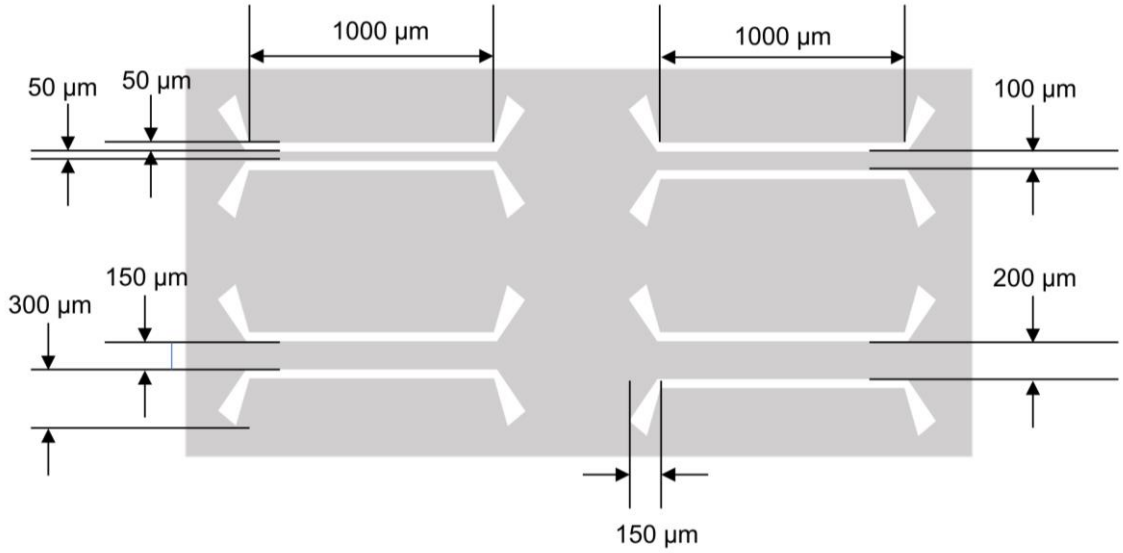

Supplementary Fig. 37 | Photomask design for the micropatterning conductive pathways in CP-PVA organogels. The photomask with this design was used to generate the conductive micropatterns shown in Fig. 4c and Supplementary Fig. 36. CP-PVA organogels at State III (solid contents: ~50 wt%, relative to the total mass of organogel, CP's content: 22 wt% relative to the total mass of CP and PVA, thickness: ~75 µm) were irradiated using a continuous wave laser (wavelength: 532 nm; diameter of laser spot: 0.3 mm; power: 150 W m^{-2}) at a fixed scanning speed of 6 cm s^{-1} through a photomask. The white and grey regions denote transparent and non-transparent areas, respectively.

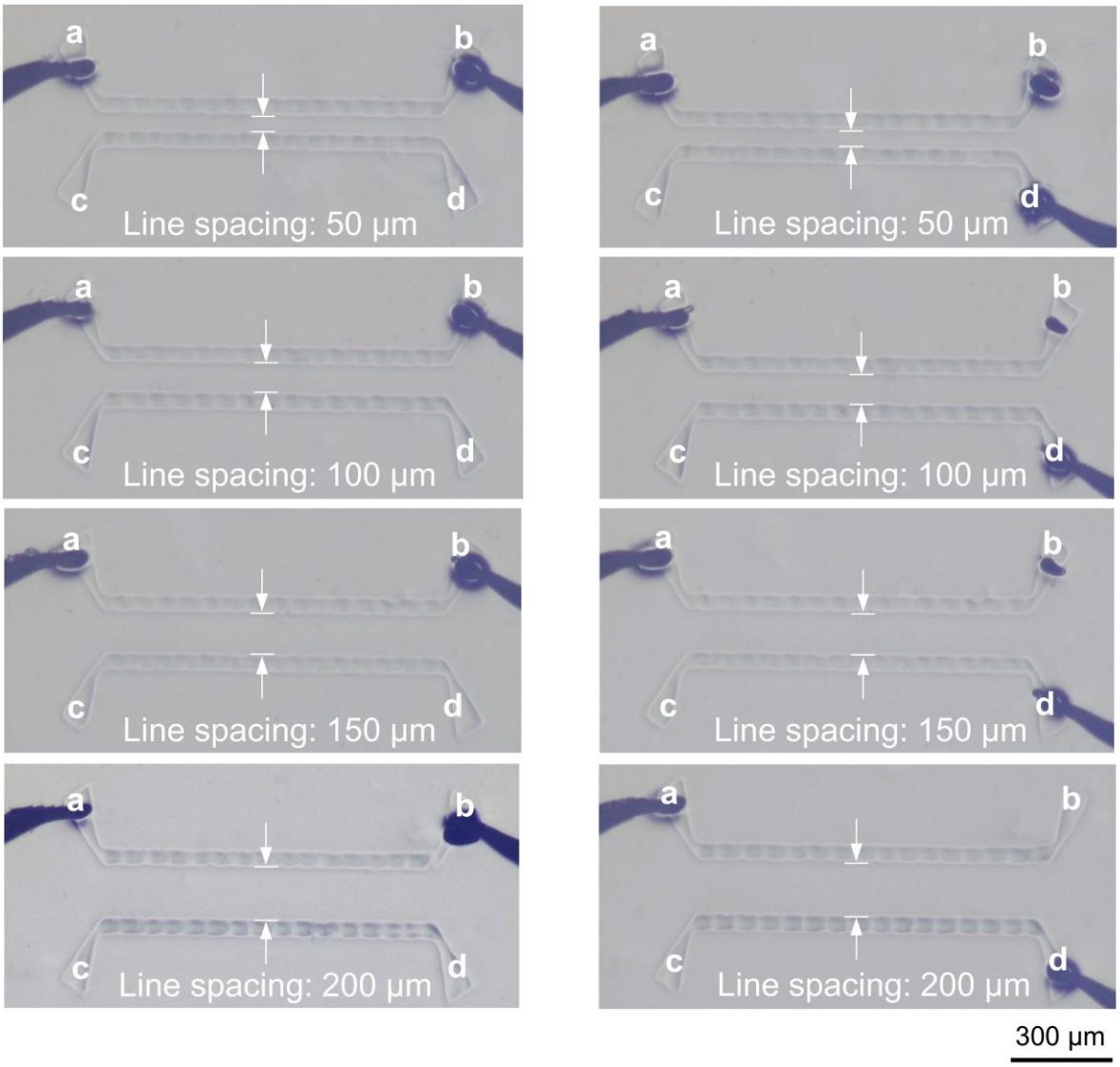

Supplementary Fig. 38 | Study on the resolution of conductive pathways through laser patterning. CP-PVA organogels at State III (solid contents: ~50 wt%, CP's relative content: 22 wt%) with a thickness of ~75 μm were irradiated with a continuous wave laser (wavelength: 532 nm, diameter of laser spot: 0.3 mm) at a fixed scanning speed of 6 cm s^{-1}, with optical power densities 150 W m^{-2}, through a photomask. Microscopic images of CP-PVA organogels patterned with different conductive pathways. The line spacing (power of laser irradiation: 150 W m^{-1}) in the conductive patterns was in the range of 50-200 μm.

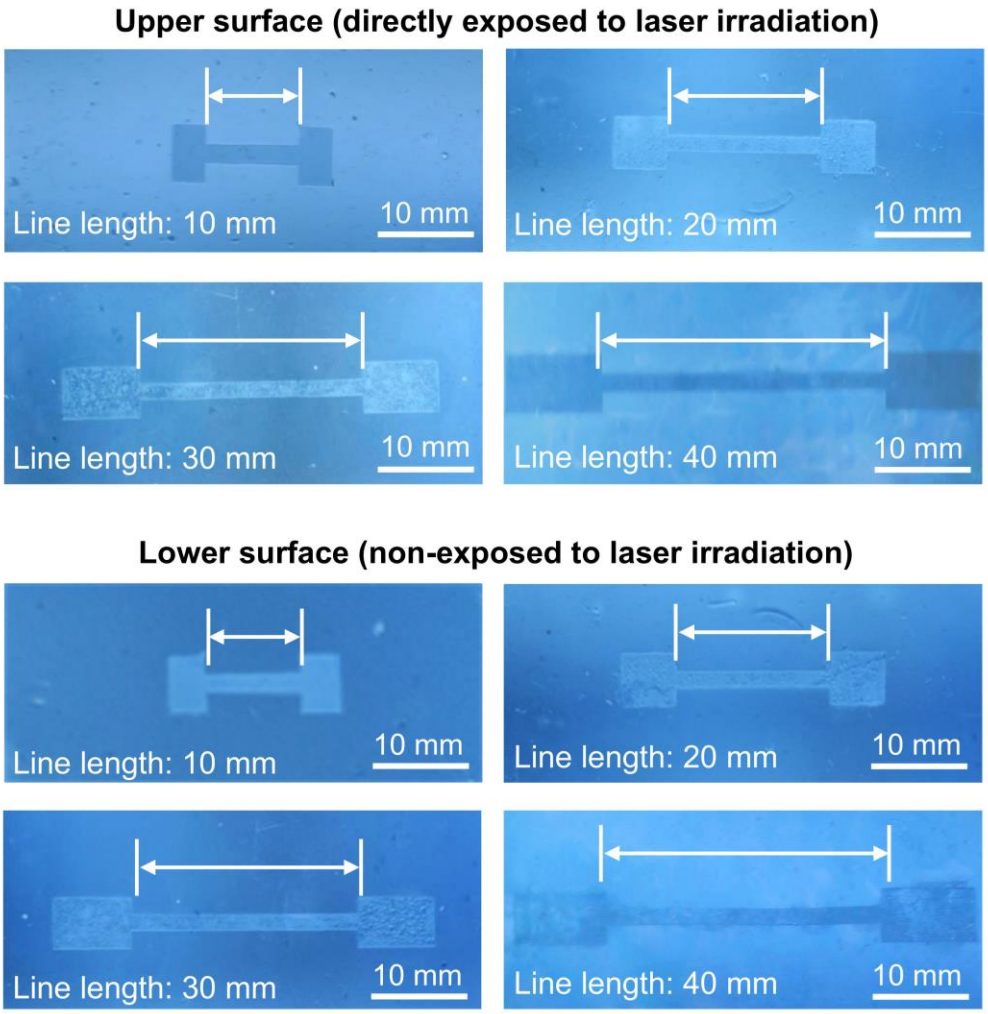

Supplementary Fig. 39 | Optical images of laser-patterned conductive pathways in CP-PVA organogel. Digital photographs of conductive traces formed within CP–PVA organogels at State III (solid contents: ~50 wt%, relative to the total mass of organogel, CP's content: 22 wt% relative to the total mass of CP and PVA, thickness: ~75 μm) via irradiation with a continuous-wave 532 nm laser (spot diameter: 0.3 mm; power: 150 W m^{-2}; scanning speed: 6 cm s^{-1}).

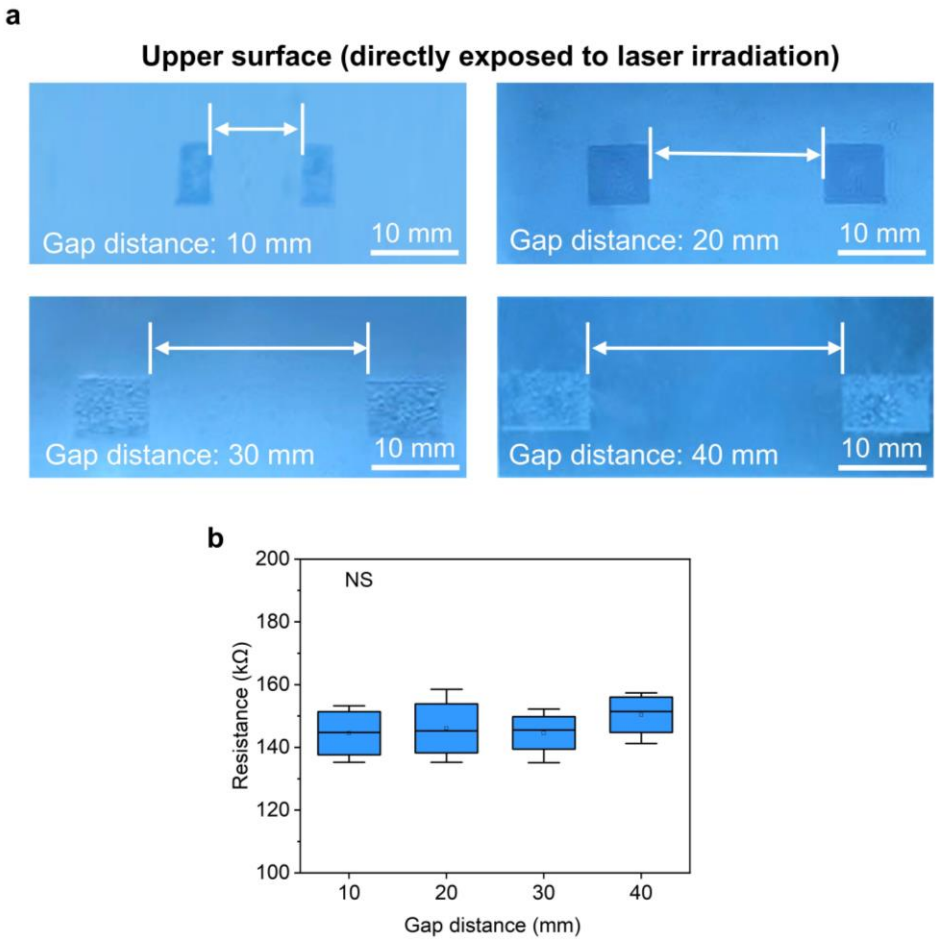

Supplementary Fig. 40 | Control experiments on laser-patterned conductive traces. a-b, compared with the dumbbell-shaped conductive traces shown in Supplementary Fig 39, only rectangular contact pads were printed through laser irradiation. The resistances between the two contact pads were 3-4 orders of magnitude higher than the values for those with conductive traces between these two pads. The data in panel **b** are presented as mean ± standard deviation (s.d.) from four independent samples. The data in panel **b** are presented in box-and-whisker plots, where the central dots, lines, and box limits indicate the mean, the median, and the upper/lower quartiles, and the whiskers extend to 1.5× the interquartile range from the quartiles. Statistical significance was assessed using one-way analysis of variance (ANOVA) for comparisons among multiple groups (panel **b**), with significance levels denoted as $p \geq 0.05$ (not significant, NS), $p < 0.05$(*), $p < 0.01$(**), and $p < 0.001$(***).

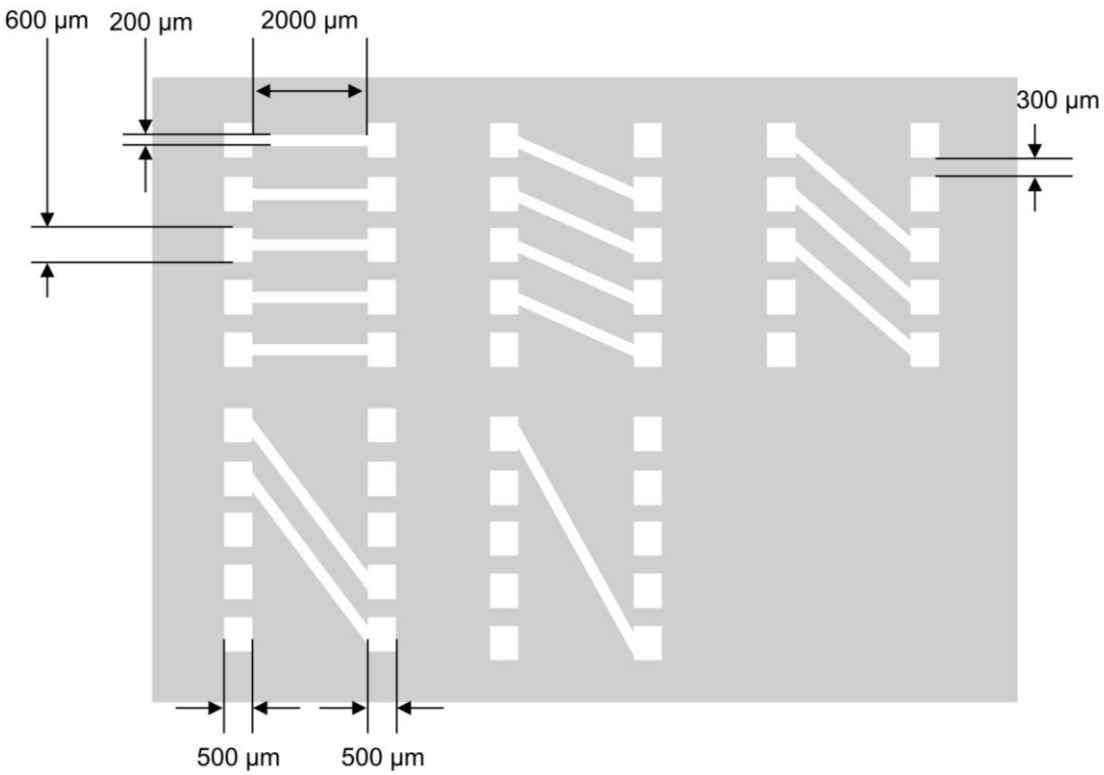

Supplementary Fig. 41 | Photomask design for the micropatterning conductive pathways in CP-PVA organogels. The photomask with this design was used to generate the conductive micropatterns shown in Fig. 4h and Supplementary Fig. 42. The white and grey regions denote the transparent and non-transparent areas, respectively.

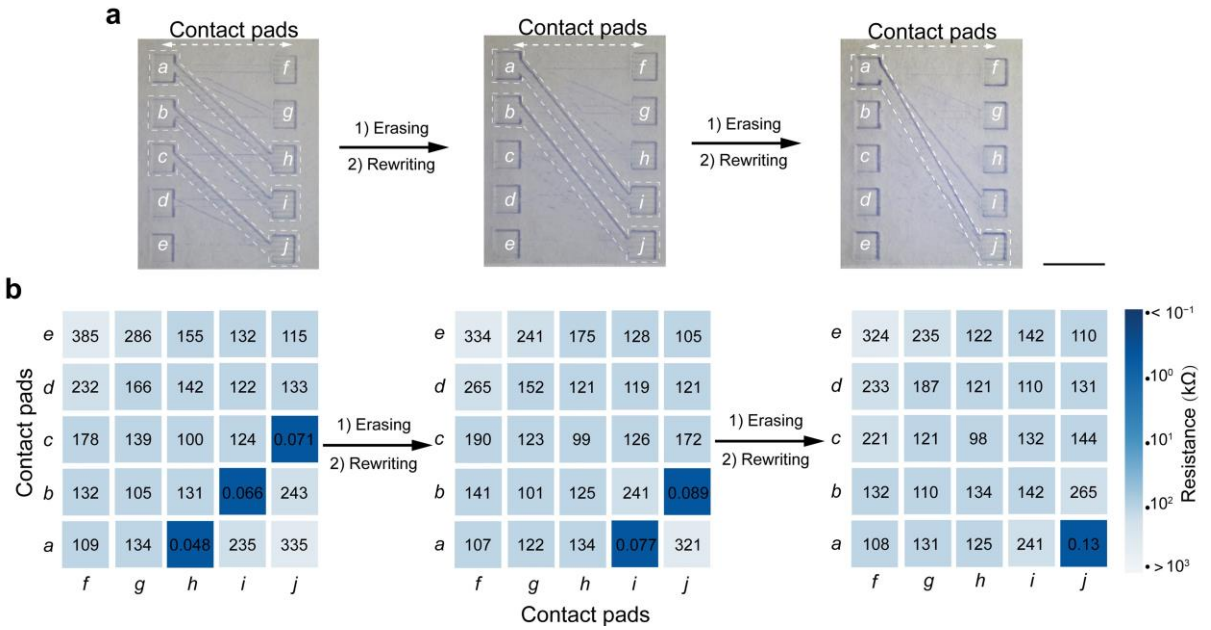

Supplementary Fig. 42 | Reconfigurability of conductive pathways patterned in a CP-PVA organogel. **a, b,** Reconfigurability of conductive traces: microscopic images of a conductive trace array fabricated within a CP-PVA organogel (scale bar, 100 μm) (**a**); summary of resistance values measured between arbitrary pair of contact pads (**b**). The area outlined with white dashed lines in the microscopic images indicates the laser-induced conductive trace.

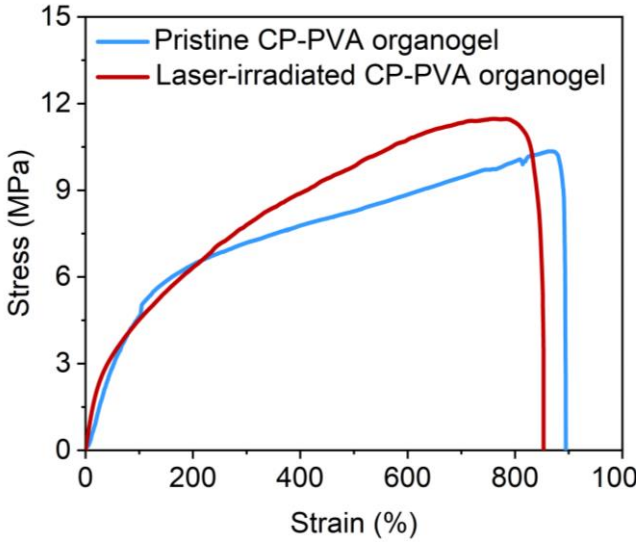

Supplementary Fig. 43 | Interfacial adhesion between laser-irradiated and non-irradiated areas of CP-PVA organogels. The CP-PVA organogels (solid contents: ~50 wt%, relative to the total mass of organogel, CP's content: 22 wt% relative to the total mass of CP and PVA, thickness: ~75 μm) were partially irradiated using a continuous wave laser (wavelength: 532 nm, diameter of laser spot: 0.3 mm) at a fixed scanning speed of 6 cm s^{-1}, with optical power densities 150 W m^{-2}. The stress-strain curves of partially laser-irradiated CP-PVA organogel were measured at a strain rate of 200% min^{-1}.

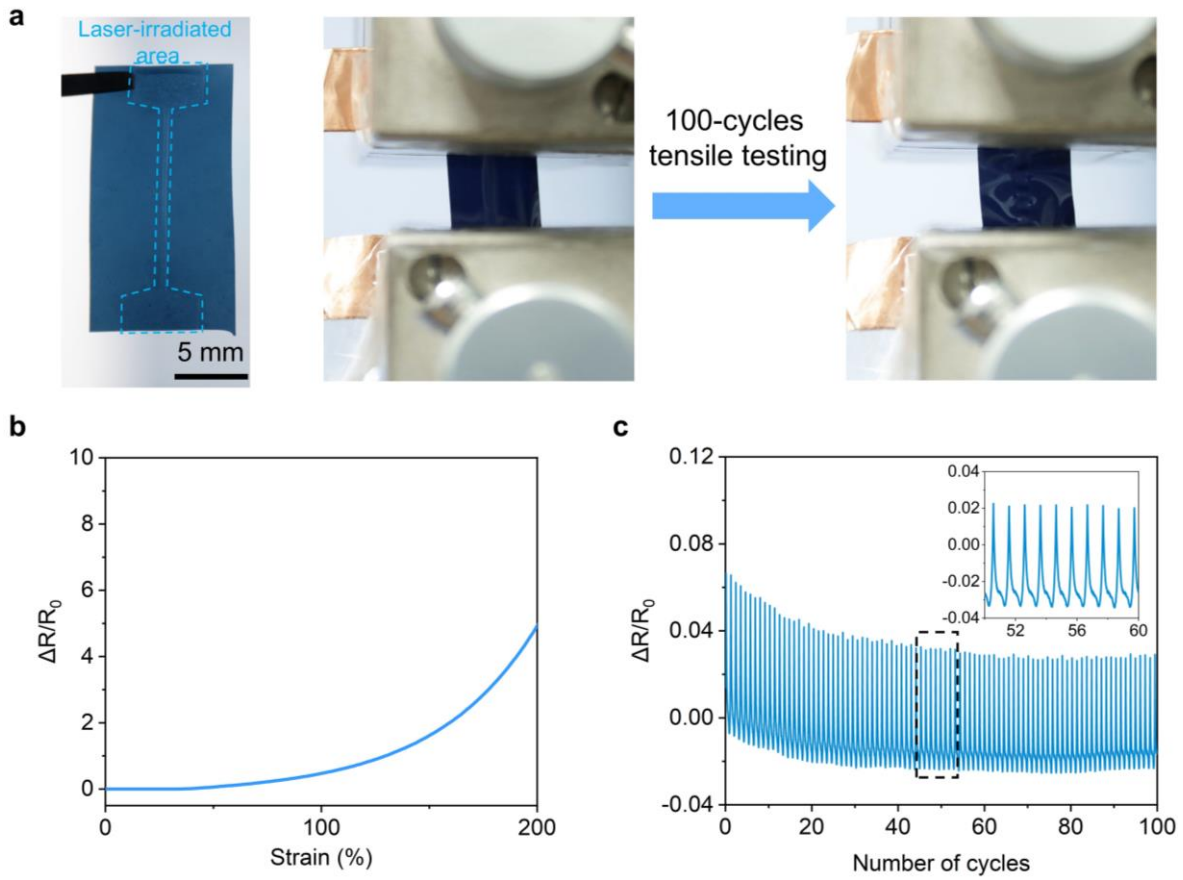

Supplementary Fig. 44 | Resistance changes of a single conductive trace patterned in a CP-PVA organogel under tensile strain. **a,** Digital photograph of CP-PVA organogels with a dumbbell-shaped conductive trace. **b, c**, Resistance change of the conductive trace upon tensile strain. The CP-PVA sample was connected to a digital source meter through a conductive copper tape coated with silver paste, and the resistance was measured at a constant-current mode (100 μA) when the sample was being stretched up to 200% at a strain rate of 200% min^{-1} (**b**) or subject to cyclic tensile test within a strain range of 0-50% at the same rate (**c**).

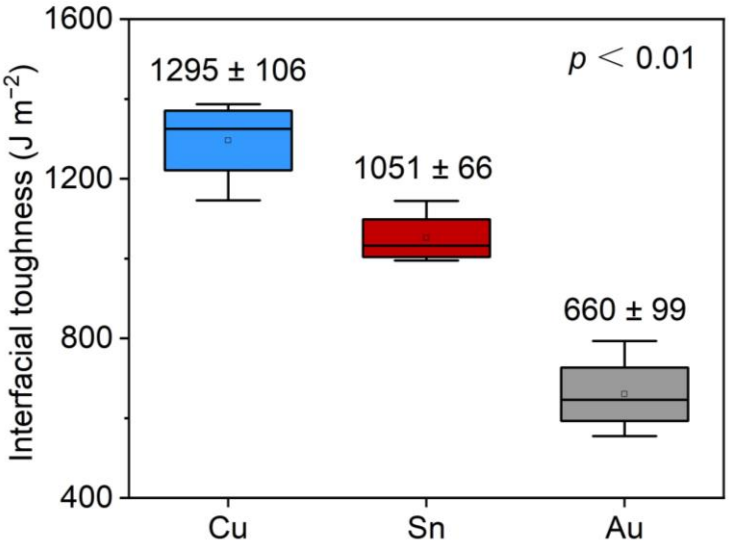

Supplementary Fig. 45 | Interfacial adhesion between CP-PVA organogels and metal substrates using CP/PVA aqueous solder. Summary of interface toughness values for CP-PVA organogels(solid content: ~50 wt%; CP's content: 22 wt% relative to the total mass of CP and PVA) adhered to Cu, Sn, and Au substrates using CP/PVA aqueous solder (solid content: 3.6 wt%, CP's content of 22 wt% relative to the total mass of CP and PVA). The data are presented as mean ± standard deviation (s.d.) from four independent samples. The data are presented in box-and-whisker plots, where the central dots, lines, and box limits indicate the mean, the median, and the upper/lower quartiles, and the whiskers extend to 1.5× the interquartile range from the quartiles. Statistical significance was assessed using one-way analysis of variance (ANOVA) for comparisons among multiple groups, with significance levels denoted as $p \geq 0.05$ (not significant, NS), $p < 0.05$(*), $p < 0.01$(**), and $p < 0.001$(***).

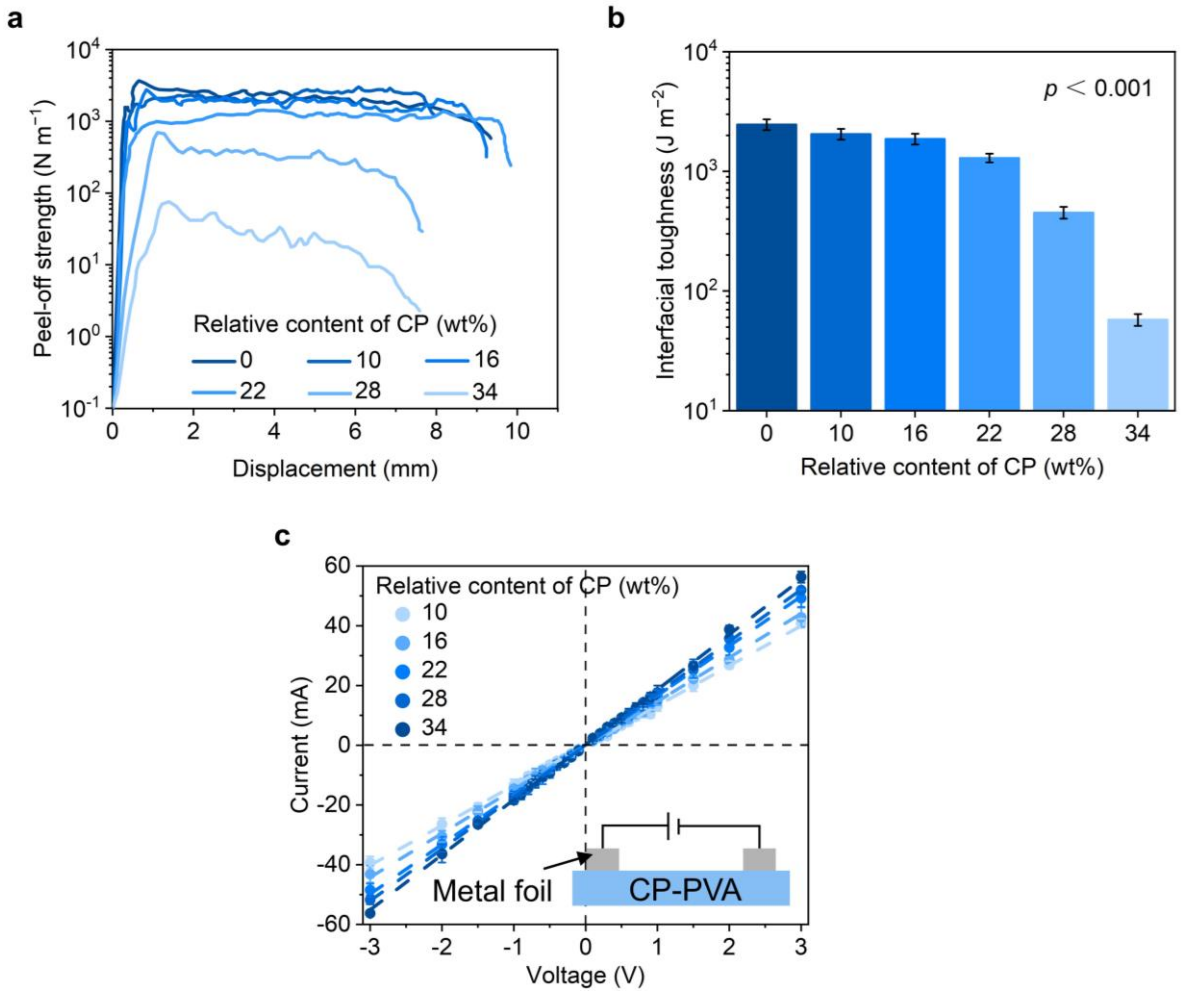

Supplementary Fig. 46 | Effect of CP content in CP/PVA aqueous solder on interfacial adhesion and electrical contact between CP-PVA organogels and Cu substrates. a-c, Force-displacement curves (**a**), interface toughness (**b,** 90° peel-off tests), and electrical contact analysis (**c**) for CP-PVA organogels adhered onto Cu substrates using CP/PVA aqueous solder with different contents of CP. The inset showed the illustrative setup for electrical contact analysis. Increasing the CP's contents in the CP/PVA aqueous solder led to a reduction in contact resistance but at the compromise of the peel-off strength particularly when the CP's relative content was lower than 34 wt%. The data in panels **b**, **c** were presented as mean values ± standard deviation (s.d.), with four different samples examined in independent measurements. Statistical significances were assessed using one-way analysis of variance (ANOVA) for comparisons among multiple groups (panel **b)**, with significance levels denoted as $p \geq 0.05$ (not significant, NS), $p < 0.05$(*), $p < 0.01$(**), and $p < 0.001$(***).

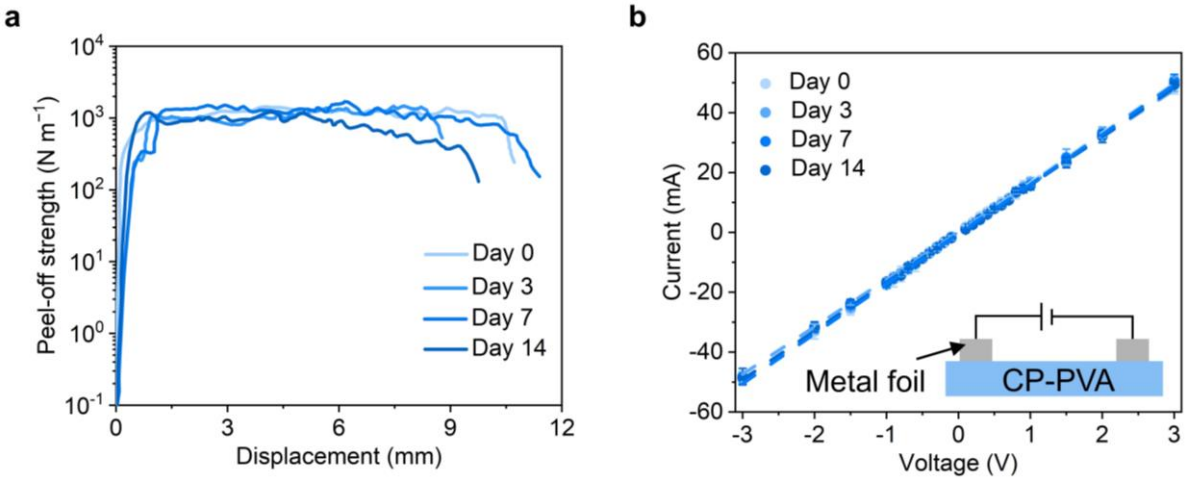

Supplementary Fig. 47 | The interfacial stability between CP-PVA organogels and Cu substrates. a, b, Force-displacement curves (**a,** 90° peel-off tests) and electrical contact analysis (**b**) for CP-PVA organogels adhered to Cu foils using CP/PVA aqueous solder (CP's content: 22 wt% relative to the total mass of CP and PVA). The inset showed the illustrative setup for electrical contact analysis. The samples were stored in an ambient environment for 0-14 days before testing. The data in panel **b** were presented as mean values ± standard deviation (s.d.), with four different samples examined in independent measurements.

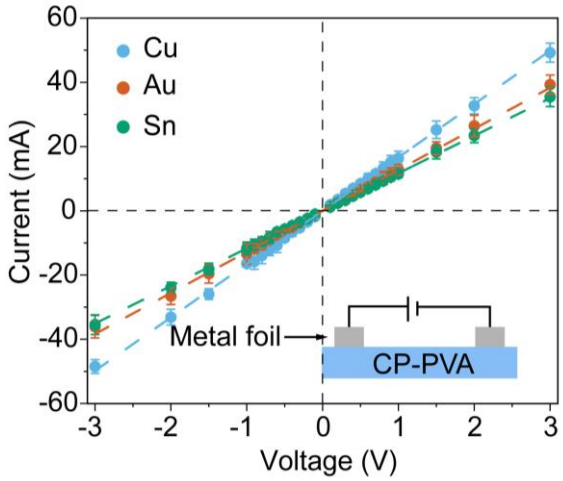

Supplementary Fig. 48 | Electrical contact between CP-PVA organogels and different metal foils with CP/PVA aqueous solder. The electrical contact analysis for CP-PVA organogels adhered to Cu, Sn, and Au substrates using CP/PVA aqueous solder (CP's content: 22 wt% relative to the total mass of CP and PVA). The inset showed the illustrative setup for electrical contact analysis. The data were presented as mean values ± standard deviation (s.d.), with four different samples examined in independent measurements.

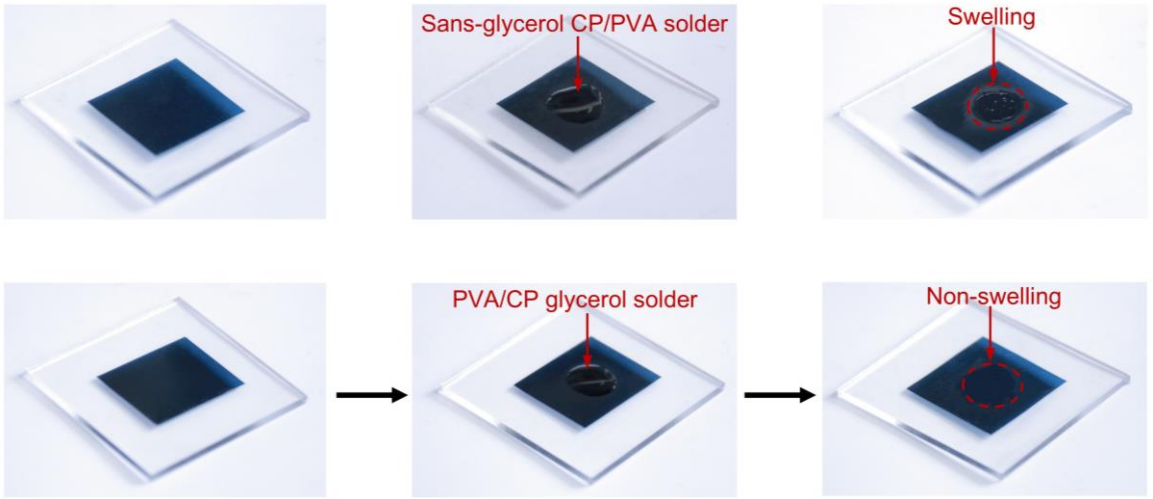

Supplementary Fig. 49 | Swelling behavior of CP-PVA organogels upon application of CP/PVA aqueous solder or CP/PVA glycerol-containing solder. The CP-PVA organogels experienced obvious swelling when being applied with CP/PVA aqueous solder (solid content: 3.6 wt%, CP's content of 22 wt% relative to the total mass of CP and PVA). In contrast, the organogels remained relatively intact when treated with CP/PVA glycerol-containing solder (the content of glycerol was 4 wt% relative to the total mass of final solution, and the concentrations of CP and PVA were 7.4 mg mL^{-1} of CP and 26.1 mg mL^{-1}) were utilized.

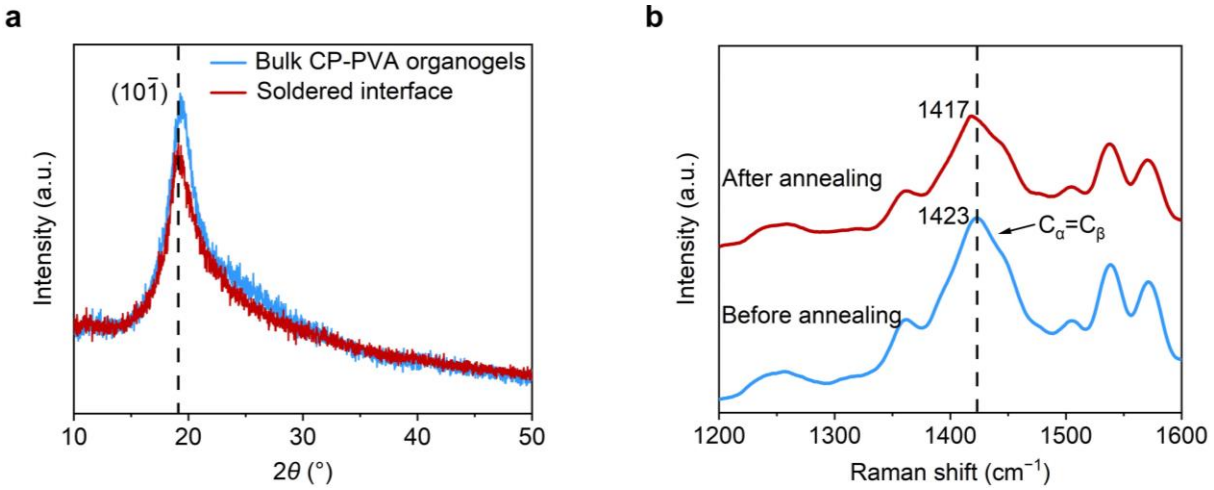

Supplementary Fig. 50 | X-ray diffraction (XRD) characterization and Raman spectra of CP-PVA organogel after wet soldering. For the soldering, CP-PVA organogels (CP's content of 22 wt% relative to the total mass of CP and PVA) were applied with a thin layer of CP/PVA aqueous solder (the concentrations of CP and PVA were 7.4 mg mL^{-1} of CP and 26.1 mg mL^{-1}), pressed against the targeted metal substrates, selectively dried overnight (for mechanical bonding), and then thermally annealed (for electrical connect) at 80 °C for 2 hours. **a,** XRD patterns of the bulk CP-PVA organogels and the soldered interface. The diffraction peaks at 19.5° were ascribed to (10$\bar{1}$) crystalline facets of PVA chains in the CP-PVA hydrogels. **b,** Raman spectra of the soldered interface of CP-PVA organogel before and after thermal annealing at 80 °C for 2 hours.

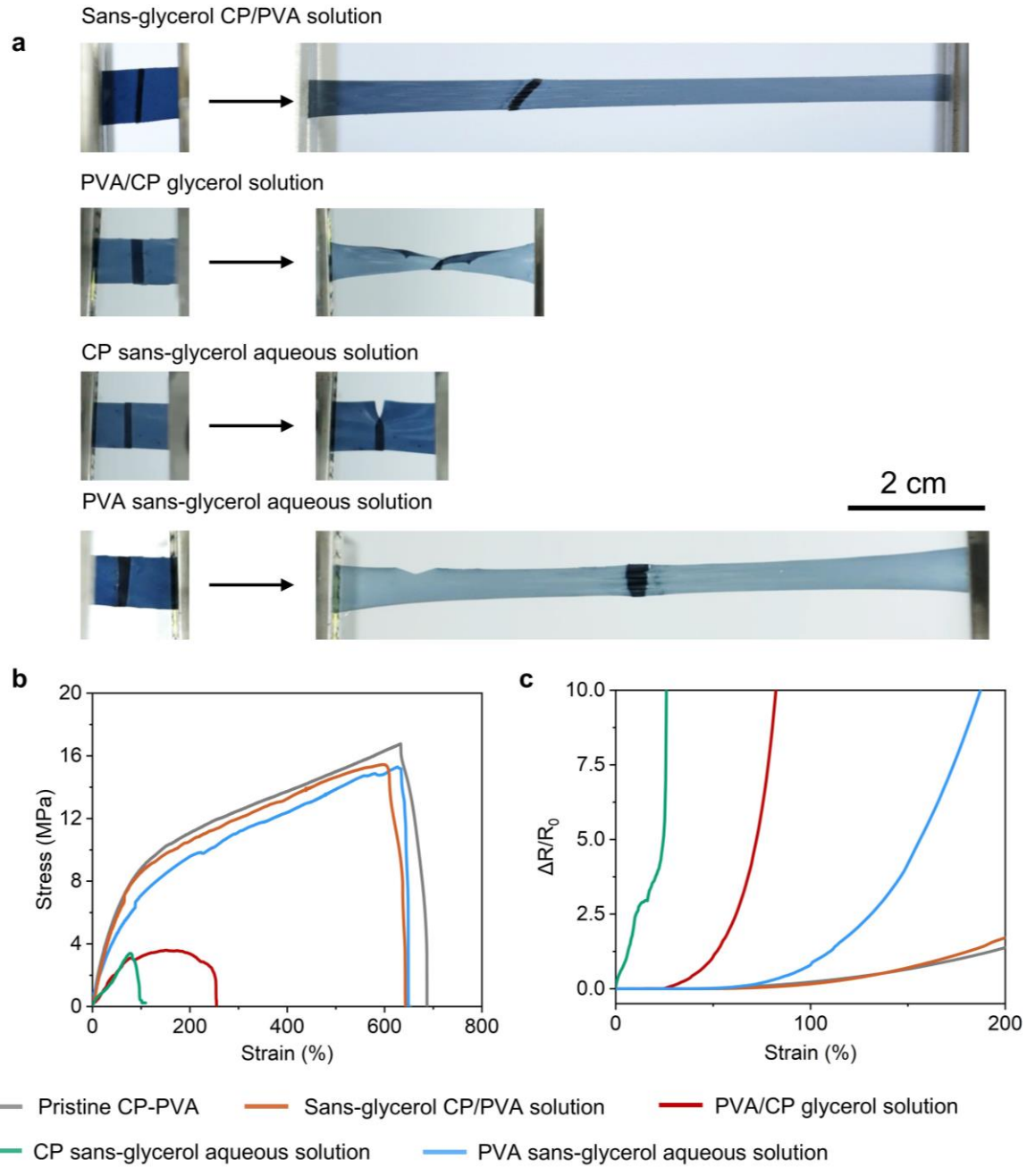

Supplementary Fig. 51 | Soldering of CP-PVA organogels with different solders. Two CP-PVA organogels were bonded together with different solders including sans-glycerol CP/PVA aqueous solder (the concentrations of CP and PVA were 7.4 mg mL^{-1} of CP and 26.1 mg mL^{-1}), CP sans-glycerol aqueous solder (1.1–1.3% solid content), PVA sans-glycerol aqueous solder (10% solid content), and CP/PVA glycerol solution solder (the content of glycerol was 4 wt% relative to the total mass of final solution, and the concentrations of CP and PVA were 7.4 mg mL^{-1} of CP and 26.1 mg mL^{-1}). For the CP/PVA glycerol solution solder, the recipe was similar to that of CP/PVA aqueous solder except that 4 wt% of glycerol was added (relative to the total mass of the solution). **a, b,** Digital photograph and stress-strain curves of soldered samples at a strain rate of 200 min^{-1}. **c,** Resistance change of the bonded samples upon being stretched at a strain rate of 200% min^{-1}. The resistance was measured at a constant current mode with an applied current of 0.1 mA.

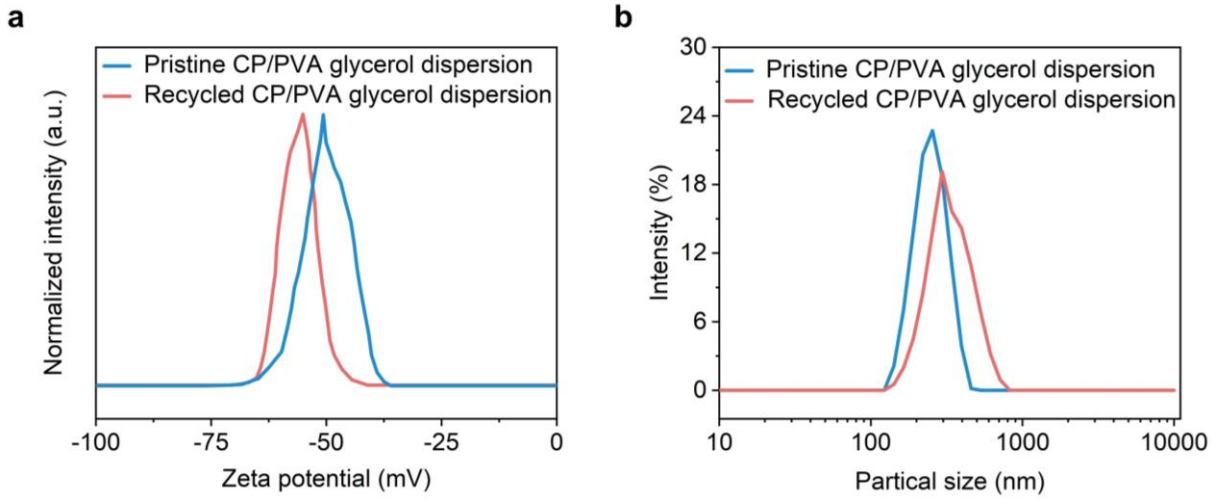

Supplementary Fig. 52 | Zeta potential and size distribution of recovered CP/PVA dispersion. For recycling, CP-PVA organogel was dialyzed with small amounts of water to remove glycerol (could be collected for subsequent use) and then dissolved in water by heating at 80 °C for 2 hours, followed by the addition of recycled glycerol (2 wt%, relative to the total mass of solution). **a, b,** Zeta potentials (**a**) and size distribution (**b**) of original CP/PVA glycerol solution and recycled CP/PVA glycerol solution.

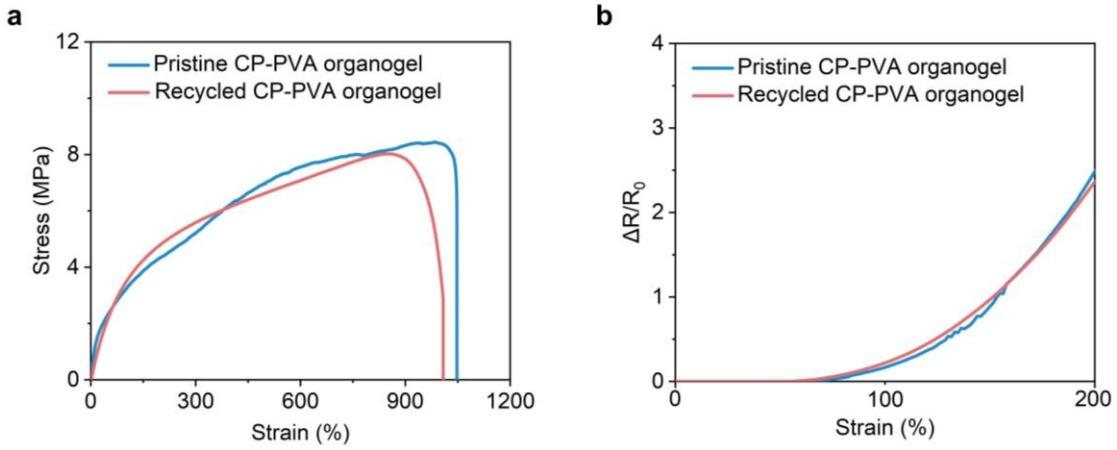

Supplementary Fig. 53 | Stress-strain curves and resistance changes of recycled CP-PVA organogels. a, Stress-strain curves of CP-PVA organogels (CP's content: 16 wt% relative to the total mass of CP and PVA) and recycled CP-PVA organogel at a strain rate of 200% min^{-1}. **b,** Resistance changes of the CP-PVA organogel and recycled CP-PVA organogel being stretched at a strain rate of 200% min^{-1}. The resistance was measured at a constant-current mode with an applied current of 0.1 mA.

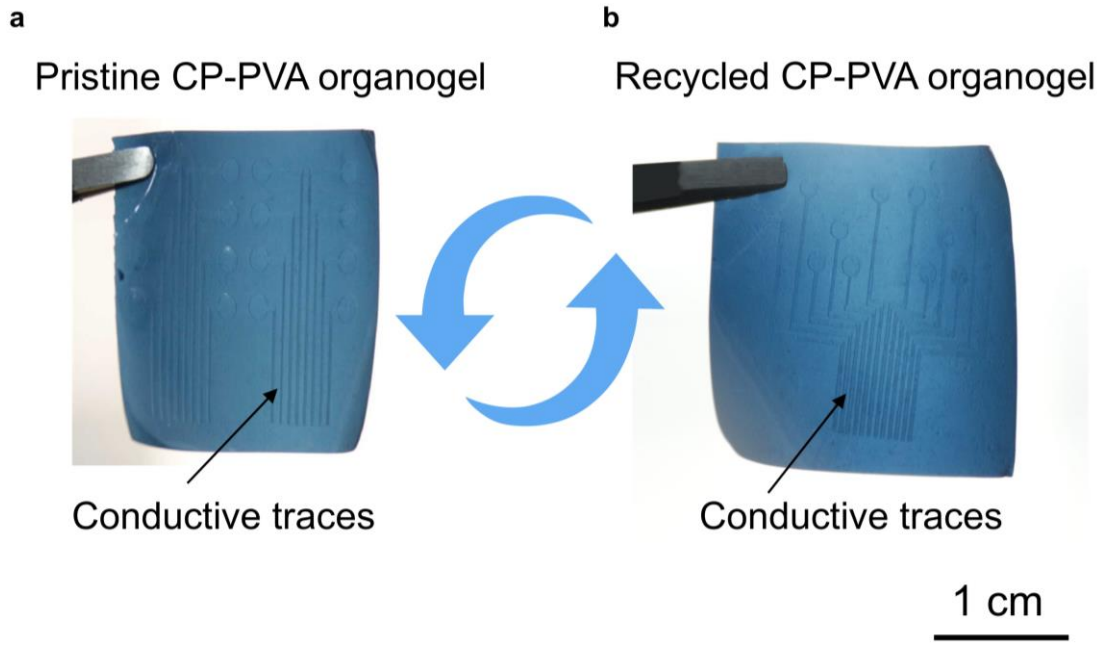

Supplementary Fig. 54 | Digital photographs of pristine and recycled CP-PVA organogel patterned with conductive traces. a-b, Enlarged digital photographs of the pristine (**a**) and recycled (**b**) CP-PVA organogels with conductive traces are shown in Fig. 5j in the main manuscript.

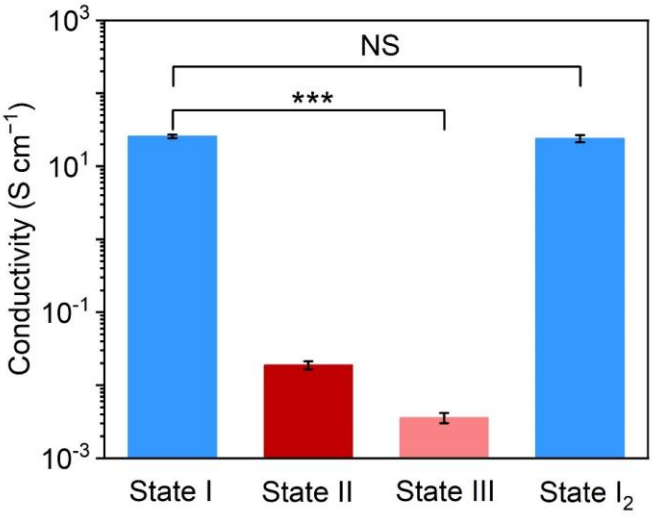

Supplementary Fig. 55 | Reconfigurability of recycled CP-PVA organogels. The recycled CP-PVA organogels (solid content: ~50 wt% relative to the total mass of organogel; CP's content: 22 wt% relative to the total mass of CP and PVA) demonstrated good electrical reconfigurability comparable to that of pristine samples, where their conductivity could be manipulated via specific ion effect as described for the pristine organogels. The data were presented as mean values ± standard deviation (s.d.), with four different samples examined in independent measurements. Statistical significance was assessed using two-sided *t*-tests for comparisons between two groups, with significance levels denoted as $p \geq 0.05$ (not significant, NS), $p < 0.05$(*), $p < 0.01$(**), and $p < 0.001$(***).

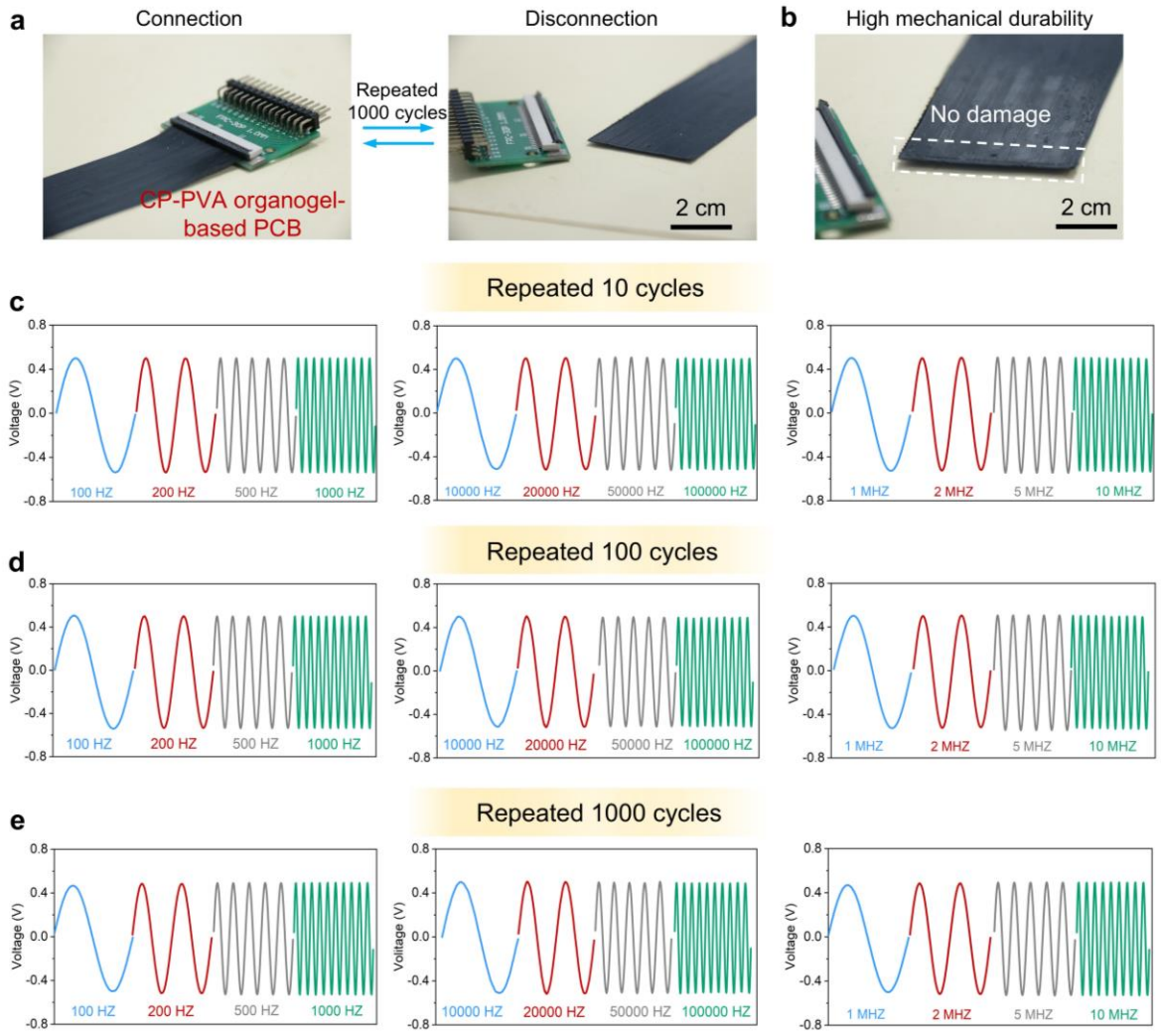

Supplementary Fig. 56 | CP-PVA organogels as 6-channels organogel-based printing circuit board (GPCB) for signal transmission. Firstly, an integrated GPCB with 6 channels was fabricated on the CP-PVA organogel at State III (CP's content of 22 wt% relatives to the total mass of CP and PVA) by a continuous-wave laser (wavelength: 532 nm, diameter of laser spot: 0.3 mm) at a fixed scanning speed of 6 cm s^{-1}. Then, GPCBs are connected to zero-insertion-force (ZIF) connectors for analog signal transmission. **a, b,** Digital photographs of CP-PVA-based PCB connection/disconnection with conventional rigid PCBs through ZIF connectors, repeated 1000 cycles. **c-e,** The GPCB connection/disconnection with ZIF connectors, repeated 10 (**c**), 100 (**d**), 1000 cycles (**e**), then analog signal transmission (range from 100 HZ-10 MHZ).

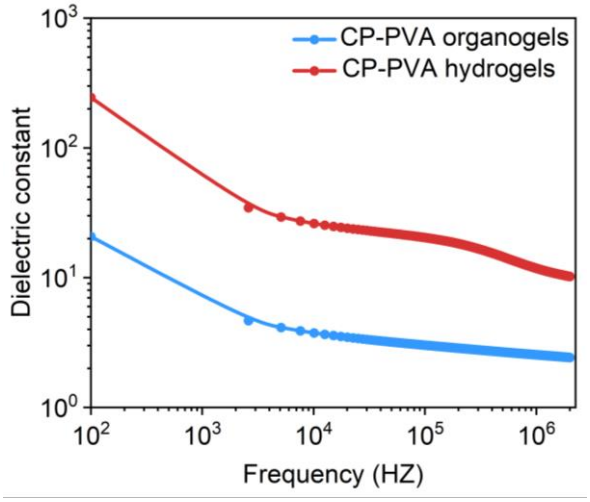

Supplementary Fig. 57 | Dielectric constants versus testing frequency for CP-PVA organogels at State III. Dielectric spectroscopy experiments were performed by a broadband dielectric spectrometer, measurements were executed at frequencies from 0.1 Hz to 20 MHz and the testing Volt root-mean-square (Vrms) was set at 1 V. The CP-PVA organogels at State III, with a solid content of ~50 wt% and CP's relative content of 22 wt%, were used for experiments. The hydrogel counterparts were prepared by dialyzing the corresponding organogels in water, followed by drying at the ambient environment (25 ℃) and reswelling in purified water. The CP-PVA organogel was soft enough to be in good contact with the testing copper electrodes with a 30 mm diameter.

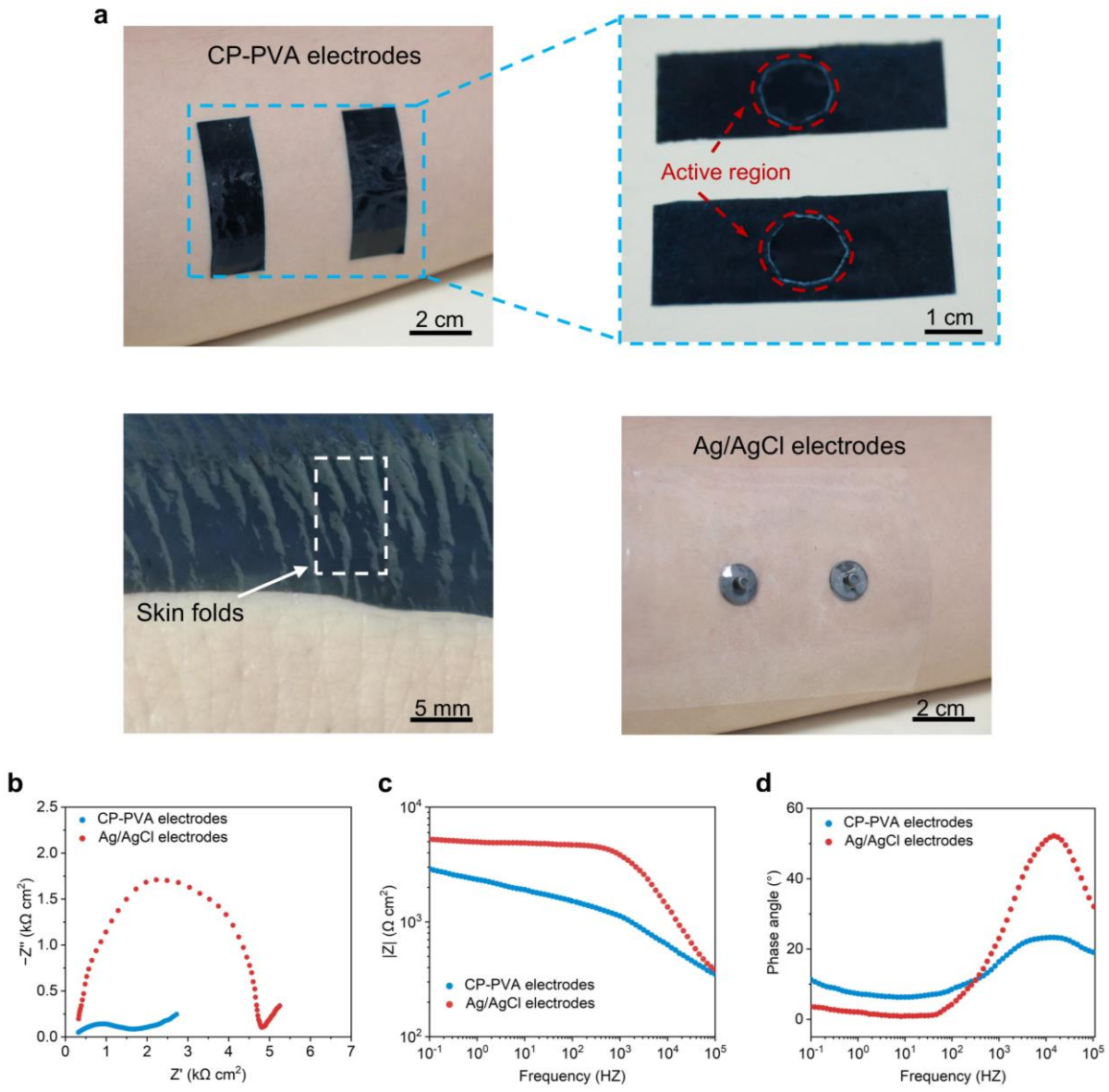

Supplementary Fig. 58 | Impedance characterizations of biological tissues. A pair of CP-PVA organogels (CP's content of 22 wt% relative to the total mass of CP and PVA) with a size of ~72 μm in thickness, 2 cm in width, and 5 cm in length was used as electrodes (the active area that contact skin: diameter 1 cm), which was then connected to an electrochemical working station. Electrochemical impedance spectra (EIS) were obtained at an initial potential of 0 V in the frequency range of 10^5–0.1 Hz. **a,** Digital photographs of CP-PVA electrodes and Ag/AgCl electrodes. **b-d,** Nyquist plots (**b**), and Bode plots (**c, d**) of CP-PVA electrodes and Ag/AgCl electrodes.

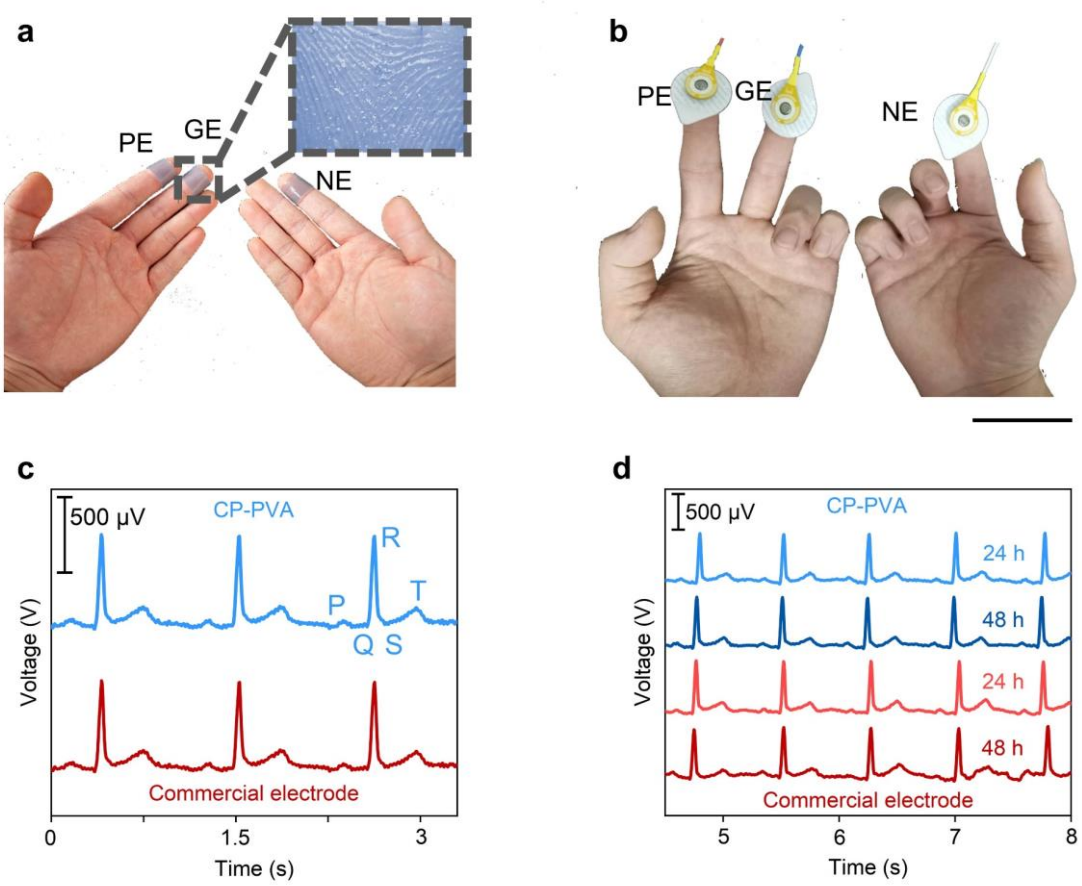

Supplementary Fig. 59 | Electrocardiogram recording by CP-PVA organogel electrodes and Ag/AgCl dry electrodes. a, b, Digital photograph depicting CP-PVA organogel electrodes (**a**) and Ag/AgCl electrodes (**b**) on fingers, indicating the good conformability of the organogels. The electrodes on the index, middle, and ring fingers of the left hand served as the positive electrode (PE), ground electrode (GE), and negative electrode (NE), respectively. **c,** Representative electrocardiography recorded by the CP-PVA electrodes, showing distinct PQRST wave peaks. The CP-PVA organogels showed a better signal-to-noise ratio than that of rigid Ag/AgCl electrodes. **d,** Continuous electrocardiogram recording monitoring by the CP-PVA over 48 hours, indicating good environmental stability.

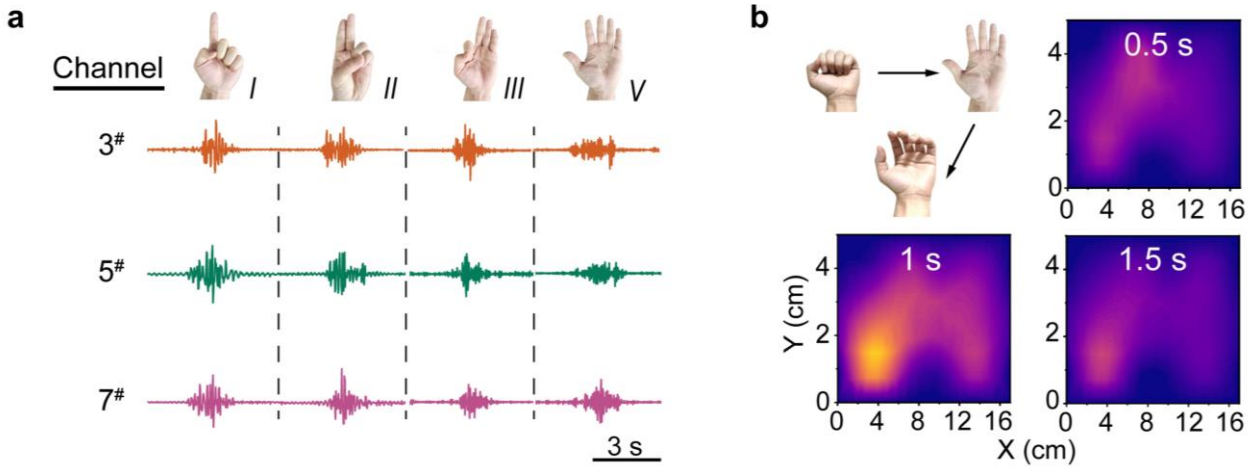

Supplementary Fig. 60 | EMG datasets of different gestures. a, Surface electromyography (sEMG) maps signals were recorded during the performance of four different gestures (gestures I, II, III, V). **b**, Temporal evolution of sEMG maps during a performance of a gesture shown in the inset. sEMG maps corresponding to the four-hand gestures were generated by calculating the root mean square (RMS) amplitude for each channel

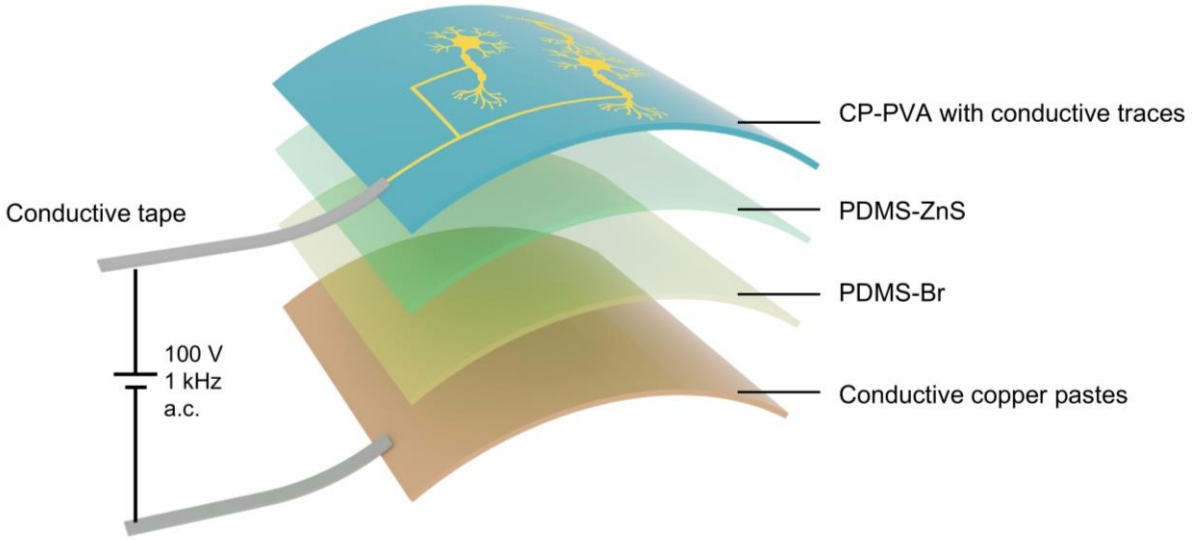

Supplementary Fig. 61 | Assembly diagram of the electroluminescent device. Which consists of a patterned CP-PVA organogel top electrode, PDMS-ZnS electroluminescent layer, PDMS-Br insulating layer, and a bottom electrode of conductive copper pastes. It is powered by a 100 V, 1 kHz a.c. supply (alternating current denoted as a.c.).

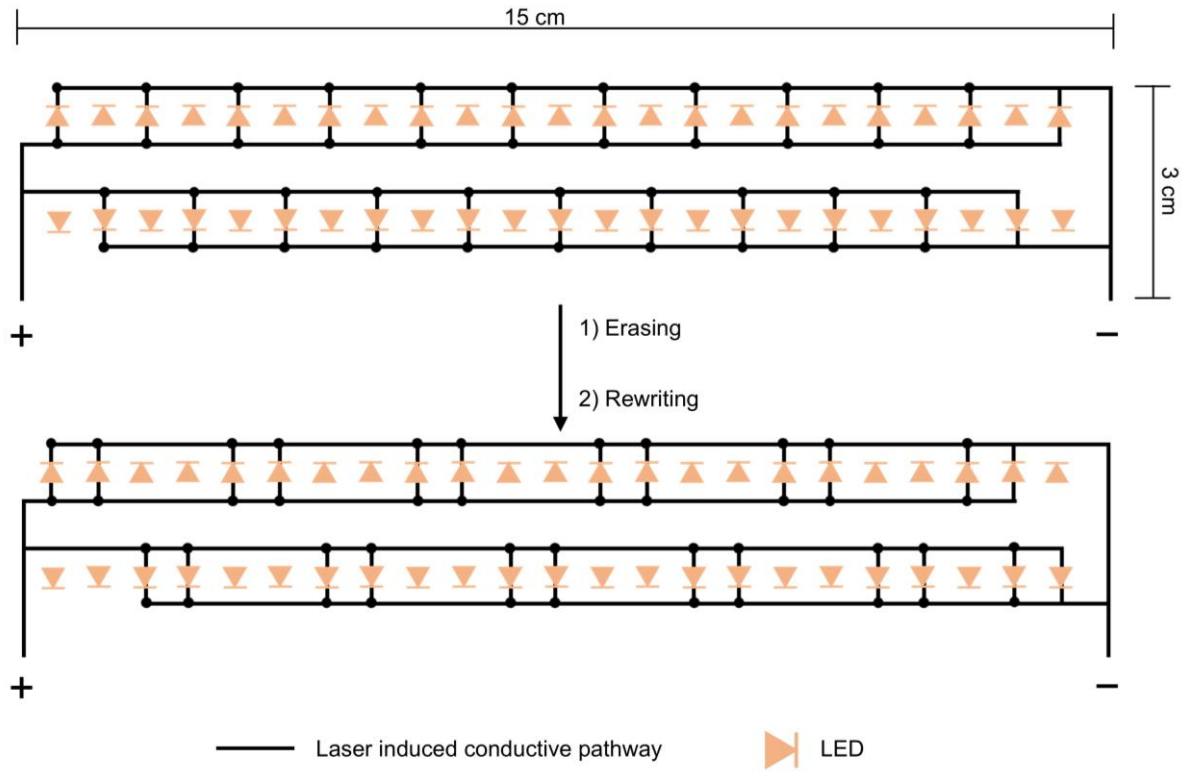

Supplementary Fig. 62 | Circuit diagram of the reconfigurable CP-PVA organogel-based LED bonds. The CP-PVA organogels at State III (solid contents: ~50 wt%, CP's relative content: 22 wt%, with a thickness of ~75 μm) were selectivity irradiated with a continuous wave laser (wavelength: 532 nm, diameter of laser spot: 0.3 mm, scanning speed: 6 cm s^{-1}, optical power densities: 150 W m^{-2}) to fabricate reconfigurable circuit. The aqueous CP/PVA solder (the concentrations of CP and PVA were 7.4 mg mL^{-1} of CP and 26.1 mg mL^{-1}) was printed onto the CP-PVA organogel through a customized stencil, serving as contact pads for LEDs. Then, the LEDs are placed on the corresponding contact pads. Finally, the LED wristbands were left at ambient temperature (~25 °C) to selectively evaporation excess water from the CP/PVA aqueous solder, and powered by a constant current of 20 mA. The conductive pathway could be erased through the treating procedure as described in the method section, and then be re-constructed through laser irradiation once again.

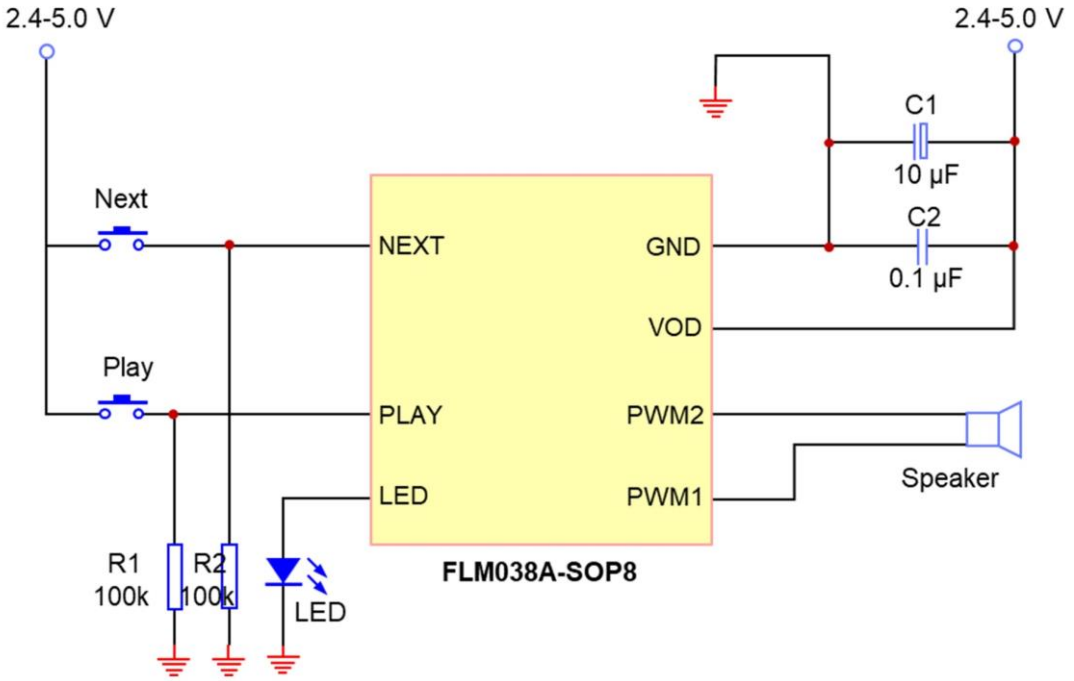

Supplementary Fig. 63 | Circuit diagram of the stretchable circuitry model for audio playing. Key components in the stretchable circuitry model include resistors, capacitors, switches, an LED, a speaker, and an FLM038A integrated circuit (IC).

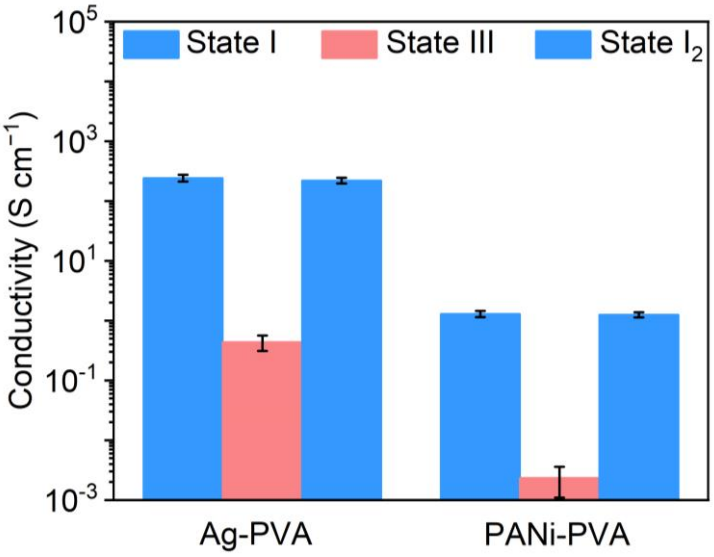

Supplementary Fig. 64 | Versatility of the reversible phase regulation strategy. The detailed preparation methods for Ag-PVA and PANi-PVA organogels are outlined in the Methods section. The pristine conductivity Ag-PVA and PANi-PVA organogels (State I) were soaked with a glycerol solution containing 2 mol L^{-1} Ca^{2+} ion for 3 days, followed by selective evaporation at an ambient environment for 24 hours (State II). For the preparation of Ag-PVA and PANi-PVA organogels at State III, the organogels at State II were dialyzed in a 15 wt% of glycerol solution for 24 hours and selectively dried at an ambient environment for 24 hours to evaporate most of the water. Then, the organogel at State III could be transformed back to State I (denoted as State I_2) through thermal annealing at 80 °C for 2 hours. The data are presented as mean values ± standard deviation (s.d.), with four samples tested in independent measurements.

Supplementary Table 1. Comparison of toughness, strain, and conductivity of CP-PVA organogel developed in this work with those of conductive hydrogel reported in previous literature.

Date	Conductive fillers	Conductivity (S cm^{-1})	Strain (%)	Toughness (MJ m^{-3})	Cited paper
	PEDOT	27.30	656	82.35	This work
		62.10	494	61.09	This work
		112.50	334	28.66	This work
1		40.00	35	0.15	3
2		6.00	290	0.07	4
3		18.50	50	0.31	5
4		10.00	150	0.62	6
5		11.00	400	2.50	7
6		0.50	500	0.19	8
7		0.11	560	0.04	9
8		0.06	750	2.63	10
9		0.01	800	1.59	11
10	Polyaniline	0.04	75	1.46	12
11		0.01	183	0.15	13
12		0.04	350	0.02	14
13		0.08	380	2.22	15
14		0.20	380	2.51	16
15	Polypyrrole	0.11	700	0.12	17
16		0.03	500	0.68	18
17		0.05	700	0.83	19
18		0.057	978	1.44	20
19	Carbon	0.062	90	0.02	21
20		0.026	433	0.13	22
21		0.0358	950	0.17	23
22		0.0487	1100	0.25	24
23		0.015	412	1.05	25

Supplementary Table 2 | FTIR spectra band assignments of PVA organogels.

Group vibration	Wavenumber value (cm^{-1})
O–H stretching	3282
C–H_2 asymmetric stretching	2939
CH_2 bending	1411
CH_2 wagging	1334
C–O stretching	1037

Supplementary Table 3 | FTIR spectra band assignments of CP organogels.

Group vibration	Wavenumber value (cm^{-1})
O–H stretching	3309
C–H_2 asymmetric stretching	2939
C=C stretching	1519
C–C stretching	1277
Sulfonic acid group	1164,
C–O stretching	1026
C-S-C stretching	952, 823 and 663

Supplementary Table 4| FTIR spectra band assignments of CP-PVA organogels.

Group vibration	Wavenumber value (cm^{-1})
O–H stretching	3263
C–H_2 asymmetric stretching	2939
C=C stretching	1519
C–C stretching	1288
Sulfonic acid group	1188
C–O stretching	1029

Supplementary Table 5. Bill of materials of organogel-based stretchable circuitry model.

Name	Parameter	Quantity
Resistance	100 kΩ	2
Capacitance	0.1 μF	1
Capacitance	10 μF	1
Speaker	—	1
Switch	—	2
LED	—	1
FLM038A	—	1

Supplemental References

1 Boehler, C. et al. Tutorial: guidelines for standardized performance tests for electrodes intended for neural interfaces and bioelectronics. *Nat. Protoc.* **15**, 3557-3578 (2020).

2 Hu, R. et al. High-fidelity bioelectrodes with bidirectional ion–electron transduction capability by integrating multiple charge-transfer processes. *Adv. Mater.* **36**, 2403111 (2024).

3 Lu, B. et al. Pure PEDOT:PSS hydrogels. *Nat Commun* **10**, 1043 (2019).

4 Yang, M. et al. Robust neural interfaces with photo patternable, bioadhesive, and highly conductive hydrogels for stable chronic neuromodulation. *ACS Nano* **17**, 885–895 (2023).

5 Yu, J. et al. Design of highly conductive, intrinsically stretchable, and 3D printable PEDOT:PSS hydrogels via PSS-chain engineering for bioelectronics. *Chem. Mater.* **35**, 5936-5944 (2023).

6 Li, G. et al. Highly conducting and stretchable double-network hydrogel for soft bioelectronics. *Adv Mater* **34**, e2200261 (2022).

7 Zhou, T. et al. 3D printable high-performance conducting polymer hydrogel for all-hydrogel bioelectronic interfaces. *Nat. Commun.* **22,** 895–902 (2023).

8 Yao, B. et al. Hydrogel ionotronics with ultra-low impedance and high signal fidelity across broad frequency and temperature ranges. *Adv. Funct. Mater.* **32**, 2109506 (2021).

9 Xue, P. et al. Highly conductive MXene/PEDOT:PSS-integrated poly(N-Isopropylacrylamide) hydrogels for bioinspired somatosensory soft actuators. *Adv. Funct. Mater.* **33**, 2214867 (2023).

10 Peng, Y., Tang, S., Wang, X. & Ran, R. A high strength hydrogel with a core-shell structure simultaneously serving as strain sensor and solar water evaporator. *Macromol. Mater. Eng.* **306**, 2100309 (2021).

11 Ji, H. et al. Sensitive wearable strain sensor based on a self-doped conductive hydrogel. *ACS Appl. Electron. Mater.* **6**, 4619-4629 (2024).

12 Qian, C. et al. A stretchable and conductive design based on multi-responsive hydrogel for self-sensing actuators. *Chem. Eng. J.* **454**, 140263 (2023).

13 Liu, Y., Jiang, D., Wu, Z., Jiang, B. & Xu, Q. Highly conductive and sensitive acrylamide-modified carboxymethyl cellulose/polyvinyl alcohol composite hydrogels for flexible sensors. *Sens. Actuators, A* **370,** 115258 (2024).

14 Du, J. et al. Robust conductive nanocomposite hydrogels with an interpenetrating network based on polyaniline for flexible supercapacitors. *Polym. Eng. Sci.* **64,** 749-760 (2023).

15 Sun, X., Zhong, W., Zhang, Z., Liao, H. & Zhang, C. Stretchable, self-healable and anti-freezing conductive hydrogel based on double network for strain sensors and arrays. *Mater. Sci.* **57,** 12511-12521 (2022).

16 Li, L. et al. Cryopolymerization enables anisotropic polyaniline hybrid hydrogels with superelasticity and highly deformation-tolerant electrochemical energy storage. *Nat. Commun.* **11,** 62 (2020).

17 Cheng, Y., Ren, X., Duan, L. & Gao, G. A transparent and adhesive carboxymethyl cellulose/polypyrrole hydrogel electrode for flexible supercapacitors. *J. Mater. Chem. C* **8,** 8234-8242 (2020).

18 Zhang, S. et al. Constructing electronic/ionic-conductive hydrogel with soft compliance and high conductivity as flexible strain sensor. *Adv. Eng. Mater.* **26,** 2400697 (2024).

19 Tie, J. et al. Nanocellulose-mediated transparent high strength conductive hydrogel based on in-situ formed polypyrrole nanofibrils as a multimodal sensor. *Carbohydr. Polym.* **273,** 118600 (2021).

20 Cao, X. et al. Hydrophobically associated hydrogel for high sensitivity and resolution of an interdigital electrode pressure sensor. *Biomacromolecules* **25,** 143-154 (2024).

21 Sun, C. et al. Highly electroactive tissue engineering scaffolds based on nanocellulose/sulfonated carbon nanotube composite hydrogels for myocardial tissue repair. *Biomacromolecules* **24,** 5989-5997 (2023).

22 Ren, J., Wang, Y., Liu, Z., Liu, K. & Xiang, X. Balancing stretchability and conductivity: carbon nanotube layer-enhanced non-ionic conductive hydrogels with a sandwich structure. *Chem. Eng. J.* **500,** 156641 (2024).

23 Youssef, A.M., Hasanin, M.S., El-Aziz, M.E.A. & Turky, G.M. Conducting chitosan/hydroxylethyl cellulose/polyaniline bionanocomposites hydrogel based on graphene oxide doped with Ag-NPs. *Int. J. Biol. Macromol.* **167,** 1435-1444 (2021).

24 Wang, Z. et al. 3D printed ultrasensitive graphene hydrogel self-adhesive wearable devices. *ACS Appl. Electron. Mater.* **4,** 5199-5207 (2022).

25 Liu, J. et al. Flexible antifreeze Zn-ion hybrid supercapacitor based on gel electrolyte with graphene electrodes. *ACS Appl. Mater. Interfaces* **13,** 16454-16468 (2021).